Reliably detecting model failures in deployment without labels

Viet Nguyen[1,2,*], Changjian Shui[1,2,*], Vijay Giri[3],
Siddarth Arya[1,2], Amol Verma[1,4], Fahad Razak[1,4], Rahul G. Krishnan[1,2]

[1] The University of Toronto, Toronto, Canada
[2] Vector Institute, Toronto, Canada
[3] University of Pennsylvania, Philadelphia, USA
[4] Unity Health Toronto, Toronto, Canada

Abstract

The distribution of data changes over time; models operating operating in dynamic environments need retraining. But knowing when to retrain, without access to labels, is an open challenge since some, but not all shifts degrade model performance. This paper formalizes and addresses the problem of post-deployment deterioration (PDD) monitoring. We propose D3M, a practical and efficient monitoring algorithm based on the disagreement of predictive models, achieving low false positive rates under non-deteriorating shifts and provides sample complexity bounds for high true positive rates under deteriorating shifts. Empirical results on both standard benchmark and a real-world large-scale internal medicine dataset demonstrate the effectiveness of the framework and highlight its viability as an alert mechanism for high-stakes machine learning pipelines.

1 Introduction

Performance guarantees of conventional machine learning (ML) models hinge on the belief that the distribution of data with which these models train is identical to the distribution on which they are deployed [1, 2, 3]. In many real-world scenarios such as healthcare, however, this assumption fails due to distribution shift during model deployment. Benchmarks such as WILDS [4] and WILD-Time [5] have encouraged machine learning researchers to study and better understand how data shifts influence predictive systems. Yet, the number of tools at a practitioner's disposal for building predictive models far exceeds those to monitor model failures. There is a need to create *guardrails* that *self-detect* and *alert* end-users to critical changes in the model when its performance drops below acceptable thresholds [6, 7].

Post-deployment deterioration (PDD) monitoring presents a distinct set of systemic challenges stemming from considerations over the feasibility of deployment in real-world ML pipelines. Predominant is the scarcity of labels during deployment: for many downstream tasks such as in healthcare, labels are expensive to obtain [8] or require human intervention [9]. Due to deployed models predicting events temporally extended in the future [10, 11], labels might even be unavailable. Another is the robustness of the monitoring system: it should flag critical changes in model deterioration early, using few samples, while remaining resilient to non-deteriorating changes to minimize unnecessary interruptions of service among other practical considerations.

*Equal contribution, correspondence to: Viet Nguyen <viet@cs.toronto.edu>

To address these challenges, we conceive a set of desiderata for any algorithm monitoring PDD, targeting their practicality and effectiveness as plug-ins to ML pipelines. To address the scarcity of labels, PDD monitoring algorithms should operate on unlabeled data from the test distribution to ascertain potential deterioration of the deployed model. Further, PDD monitoring algorithms should not depend on training data during deployment, as continuous (even indefinite) access to sensitive or personally identifiable training data might violate certain regulations protecting the privacy of data subjects [12]. An algorithm satisfying this desideratum is scalable, as it only audits a model's input stream during monitoring with minimum data storage and regulatory concerns. Finally, PDD monitoring mechanisms should be robust to flagging non-deteriorating changes and effective in few-shot settings.

When it comes to designing monitoring protocols that satisfy the above desiderata, recent related works only partially attend to individual desiderata. The literature on distribution shifts while achieving strong empirical performance on unlabeled deployment data [13, 14, 15], are not robust to false positives when the distribution shift is non-deteriorating. The model disagreement framework [16, 17, 18, 19, 20] emerges as a competitive setup for monitoring with downstream performance considerations via the tracking of disagreement statistics, while foregoing explicit distribution shift computations. However, shift-based and disagreement-based monitoring methods all depend on the *presence of training data post-deployment*, and do not provide any guarantees on robustness against false positives in the monitoring of non-deteriorating shifts.

In this work, we answer all desiderata for PDD monitoring via the disagreement framework by proposing **D**isagreement-**D**riven **D**eterioration **M**onitoring **(D3M)**. Our contributions are as follows:

Answering desiderata. D3M is a novel algorithm operating in the label-free deployment setting (1), requiring no training data during monitoring (2), and is provably robust in flagging deteriorating shifts as well as resilient to flagging non-deteriorating shifts (3). A comparison of the satisfaction of the PDD desiderata of our method with other related work in the literature is in Table 1.

Practical and scalable. D3M is model agnostic so long as the base model's feature extractor can be optimized via gradient descent. This flexibility allows D3M to monitor various modalities of high-dimensional data. Unlike previous work, D3M avoids the retraining or finetuning of the base model via posterior sampling, crucial for the efficient monitoring of large models. Finally, owing to the decoupling of the algorithmic protocol into two distinct stages, D3M is *efficiently scalable in the size of the training dataset*, a critical consideration on the feasibility of its application onto current ML pipelines that is not enjoyed by standard baselines.

Empirical validation. We showcase experimental results on various shift scenarios in the UCI Heart Disease dataset [21], CIFAR-10/10.1 [2], Camelyon17 (WILDS) [4], and an Internal Medicine (IM) dataset[1] to demonstrate its effectiveness in monitoring models of various modalities. Our method effectively detects deployment-time deterioration with low false positive rates (FPR) when shifts are non deteriorating, and achieves competitive true positive rates (TPR) when shifts are deteriorating compared to standard baselines. In particular, we discuss how results on the internal medicine dataset suggest D3M to be well-suited for integration into real-world clinical monitoring pipelines.

Provable algorithm. Under certain assumptions about the underlying distribution changes, D3M provably monitors model deterioration using finite samples when a deteriorating shift is present. In the presence of non-deteriorating shifts, D3M provably resists detection, thereby achieving low false positive rates.

[1]For the moment, we have anonymized the name of the dataset and will be henceforth referred to as the Internal Medicine (IM) dataset.

Table 1: Comparisons between related work. *Training data-free*: whether post-deployment monitoring requires training data; *Deteriorating*: whether the method provably monitors the deteriorating shift; *Non-deteriorating*: whether the method is provably robust in the non-deteriorating shift; *Disagreement*: whether the method is based on the disagreement framework.

	Training data-free	Deteriorating	Non-deteriorating	Disagreement
Yu and Aizawa, 2019 [16]	✓	✗	✗	✓
Liu et. al., 2020 [13]	✗	✗	✗	✗
Jiang et. al., 2021 [18]	✗	✗	✗	✓
Zhao et. al., 2022 [14]	✗	✗	✗	✗
Rosenfeld and Garg, 2023 [20]	✗	✓	✗	✓
Ginsberg et. al., 2023 [19]	✗	✓	✗	✓
D3M (ours)	✓	✓	✓	✓

2 Background and Algorithm

2.1 Problem setup

Assume a base model f is supervisedly trained to classify inputs $x \in \mathcal{X}$ into finite discrete classes $\mathcal{Y} = \{1, \ldots, C\}$ from training examples $\mathcal{D}^n = \{x_i, y_i\}_{i=1:n}$ where tuples $(x_i, y_i)_{i=1:n} \sim \boldsymbol{P}^n$ for all $i \in [n]$. For a joint distribution $\boldsymbol{P}$ over $\mathcal{X} \times \mathcal{Y}$, let $\boldsymbol{P}_x$ denote its marginal distribution over $\mathcal{X}$. We are interested in designing a mechanism such that upon seeing a collection of unlabeled inputs $\{x'_i\}_{i=1:m}$ sampled from a deployment distribution $\boldsymbol{Q}_x$, the mechanism flags model deterioration if $\boldsymbol{Q}_x \neq \boldsymbol{P}_x$ **and** f underperforms on $\boldsymbol{Q}_x$ without being able to observe labels for $\boldsymbol{Q}_x$. On the other hand, if $\boldsymbol{Q}_x \neq \boldsymbol{P}_x$ while f remains performant on $\boldsymbol{Q}_x$, the mechanism should resist flagging. Achieving so ensures that our mechanism only flags deployment-time changes that are truly deteriorating.

How can we monitor ML models for deployment deterioration due to distribution shift without indiscriminately flagging any changes in the data?

We require a computable quantity ϕ, independent of labels, whose value statistically differs in-distribution (ID) and out-of-distribution (OOD) if and only if model deterioration occurs. Equipped with such, monitoring regresses to recording baseline values for ϕ evaluated on ID held-out validation samples. Then, upon collecting unsupervised deployment samples from an unknown distribution, the monitoring mechanism computes $\tilde{\phi}$ and compares it to the recorded baseline values, and finally outputs a verdict.

Leveraging insights from [16, 22, 19], the framework of model disagreement possesses this property under certain assumptions about the underlying distribution change (see Appendix A). We say that two models h_1 and h_2 disagree on an input $x \in \mathcal{X}$ if $h_1(x) \neq h_2(x)$. In particular, models are found to exhibit greater predictive disagreement on unsupervised samples that lead to model deterioration, compared to in-distribution (ID) samples. This is observed through the increased entropy-based discrepancy between classification heads in [16], or maximum disagreement between models in the same ensemble in [22] and [19], as signal for detecting deployment deterioration. Maximizing classification head discrepancy for OOD detection [16] is efficient for monitoring at deployment time since only a forward pass through the classification neural network is required to effectively output a verdict. However, this trades off classification accuracy as this training procedure alters the original trained decision boundaries. On the other hand, computing model disagreement between ensembles [19] requires finetuning a potentially large network to collect ID and deployment-time disagreement statistics ϕ. In addition, ID training data is required at deployment, further limiting the scalability of such framework.

2.2 Overview of D3M

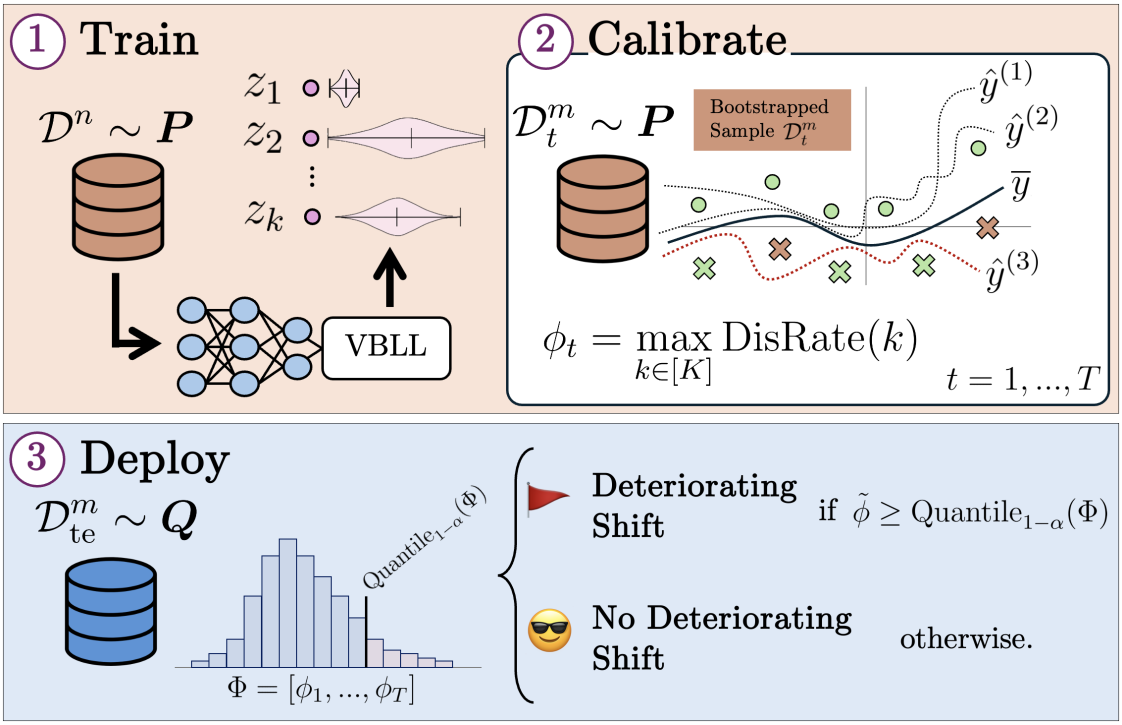

Figure 1: Overview of D3M. (1) Train: a feature extractor (FE) and a Variational Bayesian Last Layer (VBLL) are trained to model a posterior predictive distribution (PPD) over class logits. **(2) Calibrate:** disagreement statistics are computed by bootstrapping held-out ID datasets, sampling from the learned posteriors, and comparing sampled predictions to the base model's outputs to collect a set of maximum disagreement rates Φ. For illustrative purposes, agreements and disagreements between $\hat{y}^{(3)}$ and $\bar{y}$ are colored green and orange, respectively. **(3) Deploy:** at deployment, D3M monitors the model on incoming unlabeled data by computing the maximum disagreement rate $\tilde{\phi}$ and flags deteriorating shift if $\tilde{\phi} \geq \text{Quantile}_{1-\alpha}(\Phi)$.

To avoid needing the original training set at deployment, we replace finetuning with a Bayesian approach that models a posterior predictive distribution (PPD) over logits. This yields a distribution over decision boundaries that remains faithful to ID behavior. By comparing samples from the PPD to the mean prediction, we approximate maximum disagreement without retraining or access to training data. As the PPD is usually intractable, we instead model it with a variational distribution, easily optimizable using standard methods.

Sampling disagreement statistics ϕ in this way yields a reference distribution Φ of ID maximum disagreement rates. At deployment, we compute the same statistic $\tilde{\phi}$ and flag model deterioration when $\tilde{\phi}$ exceeds a high quantile of Φ. This enables unsupervised, training-free monitoring. Our method—**D**isagreement-**D**riven **D**eterioration **M**onitoring **(D3M)**—follows three key steps: **Train**, **Calibrate**, and **Deploy**.

1. (Train) Base model training. Firstly, a neural feature extractor $\text{FE}_\theta : \mathcal{X} \to \mathbb{R}^d$ coupled with a Variational Bayesian Last Layers [23] $\text{VBLL}_\theta : \mathbb{R}^d \to \mathcal{P}(\mathbb{R}^C)$ parametrized by $\theta \in \Theta$, are trained on **supervised ID** data $\mathcal{D}^n \sim \boldsymbol{P}^n$ to output posteriors over logits corresponding to C classes.

For an input $x \in \mathcal{X}$ and its ground-truth label $y \in \mathcal{Y}$:

$$\psi = \mathrm{FE}_\theta(x)$$
$$q_\theta(\cdot|x) = \mathrm{VBLL}_\theta(\psi)$$

We define our **base model** as the variational **posterior predictive distribution (PPD)** given by integrating with respect to q_θ:

$$\mathbb{P}(y|x, \mathcal{D}^n) = \mathbb{E}_{z\sim q_\theta(\cdot|x)}\left[\mathrm{softmax}(z)_y\right]$$

where predictions are assigned by computing the argmax of the PPD. Classification training is performed by maximizing the ELBO with a standard Gaussian prior $p(z)$:

$$\mathcal{L}_{\mathrm{ELBO}}(\theta; x, y) = \mathbb{E}_{z\sim q_\theta(\cdot|x)}\left[\log \mathrm{softmax}(z)_y\right] - \mathrm{KL}\left[q_\theta(z|x) \,\|\, p(z)\right]$$

2. (Calibrate) Training of ID max disagreement rates with respect to the base model. We are to gather disagreement statistics ϕ into Φ computed on ID samples for deployment time comparison. For rounds $t \in [T]$, on a held-out ID collection, we bootstrap an **unsupervised ID** dataset $\mathcal{D}_t^m = \{x_i\}_{i=1}^m \sim \boldsymbol{P}^m$ and acquire posteriors over logits $(q_\theta(\cdot|x_1), q_\theta(\cdot|x_2), \ldots, q_\theta(\cdot|x_m))$. Instead, pseudolabels $\bar{y}_i$ are assigned by the base model using the mean predictive distribution:

$$\bar{y}_i = \operatorname*{argmax}_{y=1,\ldots,C} \mathbb{E}_{z_i\sim q_\theta(\cdot|x_i)}\left[\mathrm{softmax}(z_i)_y\right], \quad \forall x_i \in \mathcal{D}_t^m$$

We draw K samples from the variational posteriors $q_\theta(\cdot|x_i)$ **in parallel** using vectorized sampling, apply a temperature-scaled softmax, and sample class labels from the resulting categorical distribution:

$$z_i^{(k)} \sim q_\theta(\cdot|x_i) \implies p_i^{(k)} \coloneqq \mathrm{softmax}\left(\frac{z_i^{(k)}}{\tau}\right), \quad \forall i \in [m], k \in [K]$$
$$\hat{y}_i^{(k)} \sim \mathrm{Categorical}\left(p_i^{(k)}\right)$$

For each posterior sample $k \in [K]$ and their corresponding predictions $(\hat{y}_1^{(k)}, \ldots, \hat{y}_m^{(k)})$, the disagreement rate of k with respect to the base model predictions $(\bar{y}_1, \ldots, \bar{y}_m)$ is calculated as:

$$\mathrm{DisRate}(k) \coloneqq \frac{1}{m}\sum_{i=1}^m \mathbb{1}\left\{\hat{y}_i^{(k)} \neq \bar{y}_i\right\}, \quad \forall k \in [K]$$

Finally, for the bootstrapped dataset $\mathcal{D}_t^m$, the maximum disagreement rate is given by:

$$\phi_t \coloneqq \max_{k\in[K]} \mathrm{DisRate}(k)$$

After T rounds, we store our collection of ID maximum disagreement rates $\Phi \coloneqq \{\phi_t : t \in [T]\}$.

3. (Deploy) Deployment monitoring of the base model. Our base model is now ready to be deployed in a test environment and outputs predictions for an unsupervised input stream. To monitor it for deployment deterioration, we periodically gather inputs into a **unsupervised** deployment dataset $\mathcal{D}_{\mathrm{te}}^m \sim \boldsymbol{Q}^m$ and compute its maximum disagreement rate $\tilde{\phi}$ as previous. D3M outputs 1 if $\tilde{\phi} \geq \mathrm{Quantile}_{1-\alpha}(\Phi)$ else 0 for a desired significance level α.

The entire protocol is summarized in Figure 1. Assume that the deployment distribution is the same as the training distribution. In this case, we expect that $\tilde{\phi} > \mathrm{Quantile}_{1-a}(\Phi)$ with probability

α, thus having immediate control over the false positive rate (FPR) of D3M. When there is, however, distribution shift between training and deployment distributions, under certain assumptions about the underlying shift and ground truth labeling, we show that D3M **provably** flags deteriorating changes, i.e. a high true positive rate (TPR) is achieved, while being resistant to flagging non-deteriorating changes, i.e. changes in the input distribution that do not result in the base model underperforming. We defer the presentation and discussion of our theoretical analysis to Appendix A.

2.3 Algorithmic insights

D3M is free from training data. D3M is designed to monitor deployment-time input streams without requiring the training data of its base model. This is an important advantage shared by [16], however not enjoyed by other baselines in Table 1, whose computation of ϕ statistics require maintaining agreement on training data. When the neural feature extractor FE is millions or billions of parameters, trained with a comparably large dataset, it becomes infeasible to store the training data within edge compute nodes in order to run the monitoring mechanism.

Prediction accuracy is preserved, metholodogy is robust to sampling. Furthermore, D3M does not trade-off prediction accuracy as the mean prediction model from the PPD is not modified during the construction of Φ nor its deployment. Therefore, ID generalization theories remain applicable [24, 25, 26, 27, 28, 29]. In addition, recording a collection of ID maximum disagreement rates reinforces the robustness of the method. While single instances of maximum disagreement rate are subject to noise in the choice of the held-out validation set, the sampling of posterior logits $z_i^{(k)}$, and the number of drawn samples K, a collection Φ of maximum disagreement rates coupled with a quantile test softens the effect of noise by leveraging large sample statistics.

Trading off Bayesian representation richness for efficiency. Harrison et. al., 2024 [23] suggests that one may apply a variational Bayesian treatment to the last layer only, saving on computational costs of forward and backward propagating through a Bayesian neural network, and enjoy largely the same uncertainty estimation and OOD detection performance. However, the usage of VBLL in D3M is unorthodox with respect to the original work: by sampling posterior weights from a Bayesian model, we are hoping to land on a set of weights such that the resulting model strongly disagree with the base model. While VBLL allows more efficient sampling compared to to a fully Bayesian network, the price to pay is the lack of diversity of the sampled predictions as the variability comes from the last layer only. This results in K sampled logits mostly agreeing with the mean prediction. To improve the diversity of sampling, we employ (1) temperature scaling and (2) the sampling of predictions from the categorical distribution for the computation of maximum disagreement rather than argmax labeling.

Potential for edge deployment. Finally, as long as the device running the monitor is able to store at least the base model (mostly the FE component), monitoring only requires forward passing batched input streams through the model and sampling logits from the last layer with additional disagreement calculations. This lightweight and purely forward-pass-based monitoring process makes D3M particularly well-suited for edge deployments, where compute and memory resources are limited. In high-stakes domains such as AI for healthcare, where on-device inference is often necessary for privacy, latency, or reliability reasons, the ability to detect distributional shift without requiring ground-truth labels or full retraining is crucial [30, 31, 32]. Similarly, in applications like insurance risk assessment or financial decision-making, where post-deployment drift can have significant regulatory or economic consequences, principled and efficient monitoring like D3M can provide an additional layer of safety and accountability [33].

2.4 Implementing D3M

The composition $\text{VBLL}_\theta \circ \text{FE}_\theta : \mathcal{X} \to \mathcal{P}(\mathbb{R}^C)$ is readily trained end-to-end on ID data of size n by maximizing the ELBO. For rounds $t \in [T]$, on a large held-out ID validation set, we sample datasets $\mathcal{D}_t^m$ of size $m \ll n$ with replacement for calibration. $\mathcal{D}_t^m$ is processed in a single forward pass, producing m independent C-dimensional Gaussian posteriors:

$$q_\theta(z_i|x_i) = \mathcal{N}(z_i|\mu_\theta(x_i), \text{diag}(\sigma_\theta^2(x_i))), \quad \text{for } i = 1, \ldots, m$$

For each posterior, we draw $2K$ samples, K for our Monte-Carlo estimation of the mean model and K for maximum disagreement computations. We keep the sampling temperature τ, the size of bootstrapped datasets m, and the number of posterior samples K as tunable hyperparameters. Importantly, these should be the exact same for the computation of Φ and the subsequent deployment-time monitoring test, where the exact same computational procedure is employed on a deployment sample $\mathcal{D}_{\mathbf{te}}^m$. A detailed implementation can be found here: https://github.com/teivng/d3m.

3 Experiments

In all experiments, at minimum, competitive performance in detecting deteriorating shifts (when present) should be achieved. This would validate D3M's effectiveness in alerting end-users of critical changes in deployment. Results on the vision datasets (CIFAR-10/10.1, Camelyon17) show that D3M is effective in monitoring high-dimensional, structure-rich data, in addition to tabular setups. Finally, we explore D3M in monitoring deteriorating and non-deteriorating changes in a real-world longitudinal electronic health record dataset (IM dataset) to study how well our method aligns with clinically meaningful degradation, bringing forth discussions on our mechanism's practical utility for trustworthy, low-intervention deployment in healthcare settings.

3.1 Experimental setup

Datasets. (1) The **UCI Heart Disease** prediction dataset [21], where each hospital corresponds to a different domain. Here, the distribution shift is due to differences in patient populations and data collection practices across hospitals. (2) **CIFAR-10/10.1** datasets [34] where shift comes from subtle changes in the dataset creation process. By viewing samples from CIFAR-10 as $\boldsymbol{P}$, we test our models' ability to flag deteriorating shift from samples in $\boldsymbol{Q}$ = CIFAR-10.1. (3) The **Camelyon17** dataset from the WILDS benchmark [4, 5] a histopathology image dataset for detecting metastases in lymph node slides, where distribution shift arises from variations in slide staining and image acquisition between hospitals contributing the data. (4) The **Internal Medicine (IM)** dataset, a comprehensive repository of standardized clinical and administrative data from hospitalizations within general internal medicine. We focus on predicting patient mortality within a 14-day horizon, leveraging static and longitudinal clinical features. This task is deemed essential for facilitating timely clinical interventions, optimizing the allocation of healthcare resources, and ultimately striving to improve patient outcomes [35, 36, 37]. Detailed data descriptions can be found in B.3. Full sweeping details and hyperparameter configurations are reported in B.5.

Implementation & Baselines. For tabular data (UCI, IM 14-day mortality), in our implementation, FE_θ corresponds to sequences of affine transformations and nonlinearities with skip-connections. For image datasets (CIFAR-10/10.1, Camelyon17), FE_θ is either a trained or a finetuned ResNet [38]. In particular, the D3M mechanism is agnostic to the choice of feature extractor, provided that the architecture reflects appropriate inductive biases for the data modality and permits gradient flow through the extracted features.

To demonstrate that our D3M enjoys low FPR on non deteriorating shifts and high TPR on deteriorating shifts, we compare it against several distribution divergence-based detection methods from the literature: Deep Kernel MMD (MMD-D) [13], H-divergence [14], Black Box Shift Detection (BBSD) [39], Relative Mahalanobis Distance (RMD) [40], Deep Ensembles [41], CTST [42], and Detectron [19]. Details can be found in Appendix B.1.

Evaluations. For all experiments, the significance level α is fixed to 0.10. (2) For UCI Heart Disease, CIFAR-10/10.1, and Camelyon17, where there are known post-deployment deterioration, we evaluate the baselines' and D3M's ability to monitor shift in $\{10, 20, 50\}$-shot scenarios. In doing so, we require that good monitors quickly recognize whether the deployment distribution has deteriorating consequences to the model or not. (3) For the IM dataset, we study the detection rates on temporally-split sub-datasets and mixtures of subpopulation splits incurring deteriorating changes and report TPR/FPR where appropriate. **For D3M, all TPRs reported are achieved while maintaining an ID FPR below α.** This is due to the temperature τ: increasing τ can cause D3M to overfit its reference disagreement distribution Φ to the held-out validation set, allowing perfect TPR but also maximal FPR.

	UCI Heart Disease			**CIFAR 10.1**			**Camelyon 17**		
	10	20	50	10	20	50	10	20	50
BBSD	.13±.03	.22±.04	.46±.05	.07±.03	.05±.02	.12±.03	.16±.04	.38±.05	.87±.03
Rel. Mahalanobis	.11±.03	.36±.05	.66±.05	.05±.02	.03±.03	.04±.02	.16±.04	.40±.05	.89±.03
Deep Ensemble	.13±.03	.32±.05	.64±.05	.33±.05	.52±.05	.68±.05	.14±.03	.26±.04	.82±.04
CTST	.15±.04	.51±.05	**.98±.01**	.03±.02	.04±.02	.04±.02	.11±.03	.59±.05	.59±.05
MMD-D	.09±.03	.12±.03	.27±.04	.24±.04	.10±.03	.05±.02	.42±.05	.62±.05	.69±.05
H-Div	.15±.04	.26±.04	.37±.05	.02±.01	.05±.02	.04±.02	.03±.02	.07±.03	.23±.04
Detectron	.24±.04	**.57±.05**	.82±.04	.37±.05	**.54±.05**	**.83±.04**	**.97±.02**	**1.0±.00**	.96±.02
D3M (Ours)	**.38±.19**	.25±.28	.69±.33	**.40±.10**	.45±.10	.74±.12	.89±.20	.93±.05	**.99±.02**

Table 2: True positive rates (TPR) comparison across datasets and query sizes. As models do experience deterioration, the higher TPR the better. **Bold** indicates best in column. We report the means and standard deviations of TPRs obtained from 10 independently seeded runs. Underlines in our results indicate that D3M is close to the best baseline.

3.2 Discussions and Analysis

UCI Heart, CIFAR-10/10.1, and Camelyon17. Model deterioration is well-known to be present, thus the **higher** reported TPR the better. Consistently, across the 3 benchmark datasets, we observe that for each of the few-shot scenarios, D3M enjoys comparable TPR to the top achieving baselines. Results on the Camelyon17 experiments at all shots highlight D3M's ability to detect diagnostically-relevant deterioration.

High-variance reported TPR and limitations. However, remarkable is the high variance of the TPRs reported on the UCI benchmark. We believe this is a shortcoming of D3M compared to the other baselines in that our few-shot results are noisier and less performant. On the one hand, there is merit in high-risk settings to flag critical changes as soon as possible. But on the other hand, more samples may be required in order to truly ascertain the deteriorating nature of a shift. It is up to users of D3M to decide the batching size of collected deployment samples depending on what provides a meaningful signal for further analyses or actionable items. This also reflects the user's tolerance for alert fatigue as noisier estimates on smaller deployment samples may get flagged more

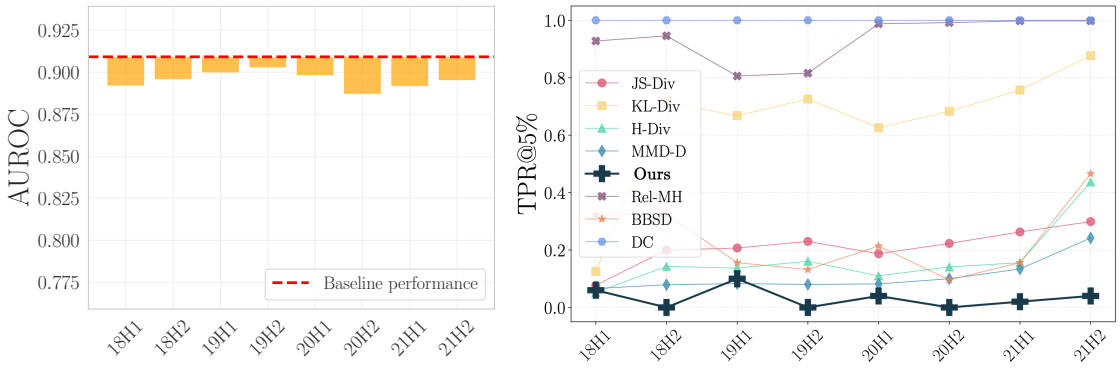

(a) Non deteriorating shift in IM **(b)** Performance monitoring

Figure 2: Performances in time evolving shifted test data from IM. **(a)** Performance drop (bar plot) is small, thus a non-deteriorating shift is observed. **(b)** Time evolving shift monitoring. D3M is robust with small False Positive Rate (FPR) at level $\alpha = 0.05$.

liberally. We discuss how selecting this deployment size implicitly allows control of the FPR of the model with additional results of D3M on bigger-shot scenarios in the above benchmarks in B.6.

Comparisons with Detectron. [19] While D3M and Detectron achieve similar monitoring performance—both successfully flagging all deteriorating shifts in higher-shot scenarios (see B.6)—D3M is significantly more scalable and practical for real-world deployment, especially at the edge. Unlike Detectron, which requires persistent access to the original training data and gradient-based finetuning during deployment, D3M operates in a truly "source-free" fashion post-training: it needs neither storage nor access to sensitive training samples, nor does it perform computationally expensive or potentially destabilizing finetuning in production. Furthermore, by relying solely on forward passes and simple statistics over deployment data, D3M is inherently robust and less susceptible to the risks associated with continual retraining, such as accidental data contamination or privacy leakage.

IM dataset results. [Temporal shift] We train the mean model on pre-2018 data and deploy on half-year splits thereafter. As shown in Fig.2(a), there is little to no performance drop over time, indicating a non-deteriorating temporal shift. Accordingly, D3M resists unnecessary alerts, maintaining a low false positive rate compared to baselines (Fig.2(b)). **[Age shift]** For deteriorating shifts, we train on adults aged 18–52 and test on various mixtures of age groups. Fig.3(a) shows a clear performance drop as more out-of-distribution samples are included. Here, all methods—including D3M—successfully flag these shifts (Fig.3(b)), with D3M achieving competitive detection across all mixture ratios. This demonstrates that D3M matches the strongest baselines in detecting genuine post-deployment deterioration. **Clinical integration and flexibility of monitoring.** In real-world clinical settings, the deployment of monitoring systems like D3M must be complemented with clear guidelines for human intervention. One practical integration point is within existing model governance frameworks in hospital information systems, where D3M's alerts could be logged and periodically reviewed by clinical data stewards or model governance committees. **Therein lies the flexibility of detecting versus agnostic adaptation**: monitoring provides a choice on what to do next given a deterioration flag, whether it be retraining, triggering deeper performance audits, shadow deployments, or even adapting. We believe D3M offers a tunable layer of oversight that can flexibly support both real-time and retrospective clinical review processes.

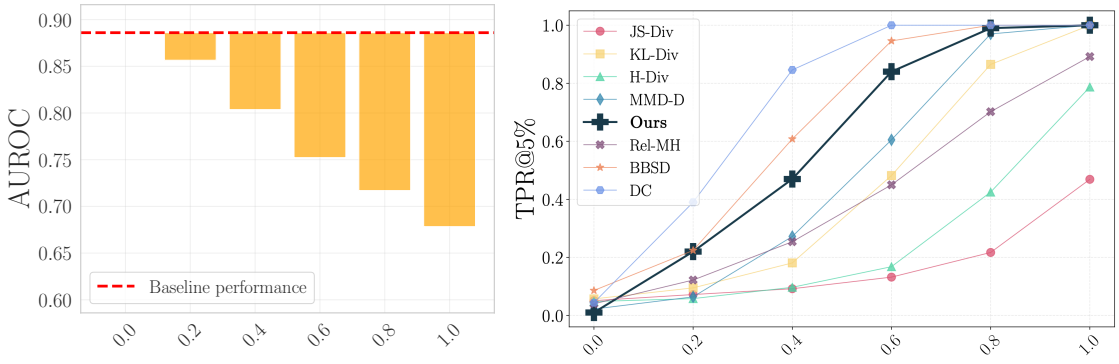

(a) Deteriorating shifts in IM **(b)** Deterioration monitoring

Figure 3: Monitoring results on artificially shifted test data from the IM dataset. **(a)** Performance drop (bar plot) is significant when the degree of shift is large ($0.0 \to 1.0$) **(b)** Results on different monitoring methods, D3M achieves competitive TPRs at level $\alpha = 0.05$.

4 Related Work

Adaptation. Test-time adaptation (TTA) concerns itself more with how one achieves strong deployment performance in spite of a critical change, rather than how one would flag this critical change. To this end, we fundamentally believe that monitoring offers an additional level of flexibility: when a deterioration flag is raised, adaptation is a possible course of action among many others. A few works from this rich body of literature are tangentially related to disagreement-based monitoring. [43, 44, 45] all leverage prediction uncertainty or discrepancy to drive unsupervised domain adaptation. [46], measures and minimizes prediction disagreement at test time, adaptively aligning target-domain features to a domain-invariant feature space, improving performance without requiring access to target domain data during training. In the continual learning literature, [47] also leverages classifier disagreement as a unsupervised proxy of distributional change.

Performance monitoring of ML models & deteriorating shift. Evaluating a model's reliability during deployment is crucial for the safety and effectiveness of the machine learning pipeline over time. [48, 49] provided a causal viewpoint wherein the challenge to adapt to diverse scenarios still remain due to a lack of access to the true causal graph. Model disagreement is often used as a monitoring tool for the model generalization [50, 17, 19, 20]. These works align strongly with our method, though the framing is orthogonal to ours as our analysis provides FPR and TPR guarantees whereas they provided sufficient conditions in either ID or other shifts beyond our scope. Several works in the recent literature differentiate shifts in terms of deteriorating or non-deteriorating shifts. [51] studied (deteriorating) shift detection in the continuous monitoring setting using a sequential hypothesis test. Due to the setting being sequential in nature, their method requires true labels from $\boldsymbol{Q}$ immediately after prediction or at the least in a delayed fashion. [52] approached the monitoring problem from a time-continuous anomaly detection perspective, allowing periodic querying of deployment-time ground truths from experts. Other related empirical works along this literature are [53, 54], and the very applied [55].

Distribution shift detection. Methods to detect distribution shift arise from different perspectives. In covariate shift detection, [42, 13, 14] treated detection as two-sample tests via classifier, Deep Kernel MMD, and H-divergence. For label shift on the other hand, [39, 56] formulated the problem as a convex optimization problem by solving the label distribution ratio $\alpha = \boldsymbol{Q}(y)/\boldsymbol{P}(y)$. The problem of OOD detection [57, 54] seeks to detect if an individual sample x comes from the

training distribution $x \sim \boldsymbol{P}(x)$. Some previous works [58, 59] also adopted the methods in covariate shift detection and generalization by estimating the density ratio for the identification of OOD samples. Whilst these methods detect shifts, they are constrained by their requirement of training data post-deployment and do not consider the extent to which shifts affect model performance.

Estimating test error with unlabeled data. Another rich body of research is the estimation of (OOD) test error. This technique and its variants are often inspired by domain adaptation theories [60, 61, 62, 63], seeking guarantess in the form of $\text{err}(f; \boldsymbol{Q}_g) \leq \text{err}(f; \boldsymbol{P}_g) + \Delta(f, \mathcal{H})$, with $\Delta(f, \mathcal{H}) = \sup_{h \in \mathcal{H}} |\text{err}(h; \boldsymbol{P}_f) - \text{err}(h; \boldsymbol{Q}_f)|$. This objective can be alternatively viewed as searching for a critic function $h \in \mathcal{H}$ to maximize a performance gap [20, 18]. One could thus provably estimate the upper bound of the test distribution error. These theories also implicitly assume the availability of training data. Further, they assume that test error should be larger than the training error (granted this is often the case for deteriorating OOD), making them sensitive to non deteriorating shifts as well i.e., a high FPR in detection. Our theoretical analysis addresses this gap.

5 Conclusion and Limitations

We study the problem of post-deployment deterioration monitoring of machine learning models in the setting where labels from test distribution are unavailable. We propose a three-stage disagreement-based Bayesian monitoring algorithm, D3M, which monitors and detects deteriorating changes in the deployment dataset while being resilient to flagging non-deteriorating changes. Importantly, our method does not require any training data during deployment monitoring, allowing for efficient out-of-the-box deployment in many machine learning pipelines across various domains. While D3M enjoys an increased in efficiency, we observe more noise between reported TPRs in independent runs, demanding stricter hyperparameter settings (and thus, bigger initial sweeps) to function effectively. Under certain assumptions, we provide statistical guarantees for low FPR in the case of non-deteriorating shifts and reliable TPR in the deteriorating shift.

Empirically, we validate insights from our theory on various synthetic and real-world vision and healthcare datasets evidencing the effective use of D3M. Our work signals a step toward the *robust, scalable, and efficient* deployment of mechanisms to audit and monitor machine learning pipelines in the break of dawn of ubiquitous AI.

References

[1] Stephan Rabanser, Stephan Günnemann, and Zachary Lipton. Failing loudly: An empirical study of methods for detecting dataset shift. *Advances in Neural Information Processing Systems*, 32, 2019.

[2] Benjamin Recht, Rebecca Roelofs, Ludwig Schmidt, and Vaishaal Shankar. Do cifar-10 classifiers generalize to cifar-10? *arXiv preprint arXiv:1806.00451*, 2018.

[3] Shibani Santurkar, Dimitris Tsipras, and Aleksander Madry. Breeds: Benchmarks for subpopulation shift. *arXiv preprint arXiv:2008.04859*, 2020.

[4] Pang Wei Koh, Shiori Sagawa, Henrik Marklund, Sang Michael Xie, Marvin Zhang, Akshay Balsubramani, Weihua Hu, Michihiro Yasunaga, Richard Lanas Phillips, Irena Gao, et al. Wilds: A benchmark of in-the-wild distribution shifts. In *International conference on machine learning*, pages 5637–5664. PMLR, 2021.

[5] Huaxiu Yao, Caroline Choi, Bochuan Cao, Yoonho Lee, Pang Wei Koh, and Chelsea Finn. Wild-time: A benchmark of in-the-wild distribution shift over time. In *Thirty-sixth Conference on Neural Information Processing Systems Datasets and Benchmarks Track*, 2022.

[6] Anand R Habib, Anthony L Lin, and Richard W Grant. The epic sepsis model falls short—the importance of external validation. *JAMA Internal Medicine*, 181(8):1040–1041, 2021.

[7] Karina Zadorozhny, Patrick Thoral, Paul Elbers, and Giovanni Cinà. Out-of-distribution detection for medical applications: Guidelines for practical evaluation. In *Multimodal AI in healthcare: A paradigm shift in health intelligence*, pages 137–153. Springer, 2022.

[8] Narges Razavian, Saul Blecker, Ann Marie Schmidt, Aaron Smith-McLallen, Somesh Nigam, and David Sontag. Population-level prediction of type 2 diabetes from claims data and analysis of risk factors. *Big Data*, 3(4):277–287, 2015.

[9] Xiaofeng Liu, Chaehwa Yoo, Fangxu Xing, Hyejin Oh, Georges El Fakhri, Je-Won Kang, Jonghye Woo, et al. Deep unsupervised domain adaptation: A review of recent advances and perspectives. *APSIPA Transactions on Signal and Information Processing*, 11(1), 2022.

[10] Noorhannah Boodhun and Manoj Jayabalan. Risk prediction in life insurance industry using supervised learning algorithms. *Complex & Intelligent Systems*, 4(2):145–154, 2018.

[11] Yuan Zhang, Xi Yang, Julie Ivy, and Min Chi. Time-aware adversarial networks for adapting disease progression modeling. In *2019 IEEE International Conference on Healthcare Informatics (ICHI)*, pages 1–11. IEEE, 2019.

[12] Rainer Mühlhoff. Predictive privacy: Collective data protection in the context of artificial intelligence and big data. *Big Data & Society*, 10(1):20539517231166886, 2023.

[13] Feng Liu, Wenkai Xu, Jie Lu, Guangquan Zhang, Arthur Gretton, and Danica J Sutherland. Learning deep kernels for non-parametric two-sample tests. In *International conference on machine learning*, pages 6316–6326. PMLR, 2020.

[14] Shengjia Zhao, Abhishek Sinha, Yutong He, Aidan Perreault, Jiaming Song, and Stefano Ermon. Comparing distributions by measuring differences that affect decision making. In *International Conference on Learning Representations*, 2022.

[15] Zhen-Yu Zhang, Zhiyu Xie, Huaxiu Yao, and Masashi Sugiyama. Test-time adaptation in non-stationary environments via adaptive representation alignment. *Advances in Neural Information Processing Systems*, 37:94607–94632, 2024.

[16] Qing Yu and Kiyoharu Aizawa. Unsupervised out-of-distribution detection by maximum classifier discrepancy. In *Proceedings of the IEEE/CVF international conference on computer vision*, pages 9518–9526, 2019.

[17] Ching-Yao Chuang, Antonio Torralba, and Stefanie Jegelka. Estimating generalization under distribution shifts via domain-invariant representations. *arXiv preprint arXiv:2007.03511*, 2020.

[18] Yiding Jiang, Vaishnavh Nagarajan, Christina Baek, and J Zico Kolter. Assessing generalization of sgd via disagreement. *arXiv preprint arXiv:2106.13799*, 2021.

[19] Tom Ginsberg, Zhongyuan Liang, and Rahul G Krishnan. A learning based hypothesis test for harmful covariate shift. In *The Eleventh International Conference on Learning Representations*, 2023.

[20] Elan Rosenfeld and Saurabh Garg. (almost) provable error bounds under distribution shift via disagreement discrepancy. *Advances in Neural Information Processing Systems*, 36, 2023.

[21] Andras Janosi, William Steinbrunn, Matthias Pfisterer, and Robert Detrano. Heart Disease. UCI Machine Learning Repository, 1989. DOI: https://doi.org/10.24432/C52P4X.

[22] Shafi Goldwasser, Adam Tauman Kalai, Yael Tauman Kalai, and Omar Montasser. Beyond perturbations: Learning guarantees with arbitrary adversarial test examples. In *Advances in Neural Information Processing Systems*, volume 33, pages 16942–16952, 2020.

[23] James Harrison, John Willes, and Jasper Snoek. Variational bayesian last layers. In *International Conference on Learning Representations (ICLR)*, 2024.

[24] Vladimir N Vapnik. An overview of statistical learning theory. *IEEE transactions on neural networks*, 10(5):988–999, 1999.

[25] Peter L Bartlett and Shahar Mendelson. Rademacher and gaussian complexities: Risk bounds and structural results. *Journal of Machine Learning Research*, 3(Nov):463–482, 2002.

[26] Chiyuan Zhang, Samy Bengio, Moritz Hardt, Benjamin Recht, and Oriol Vinyals. Understanding deep learning requires rethinking generalization. *arXiv preprint arXiv:1611.03530*, 2016.

[27] Vaishnavh Nagarajan and J Zico Kolter. Deterministic pac-bayesian generalization bounds for deep networks via generalizing noise-resilience. *arXiv preprint arXiv:1905.13344*, 2019.

[28] Yiding Jiang, Behnam Neyshabur, Hossein Mobahi, Dilip Krishnan, and Samy Bengio. Fantastic generalization measures and where to find them. *arXiv preprint arXiv:1912.02178*, 2019.

[29] Yoonho Lee, Juho Lee, Sung Ju Hwang, Eunho Yang, and Seungjin Choi. Neural complexity measures. *Advances in Neural Information Processing Systems*, 33:9713–9724, 2020.

[30] Tamra Lysaght, Hannah Yeefen Lim, Vicki Xafis, and Kee Yuan Ngiam. Ai-assisted decision-making in healthcare: the application of an ethics framework for big data in health and research. *Asian Bioethics Review*, 11:299–314, 2019.

[31] Raghubir Singh and Sukhpal Singh Gill. Edge ai: a survey. *Internet of Things and Cyber-Physical Systems*, 3:71–92, 2023.

[32] Alexandru Rancea, Ionut Anghel, and Tudor Cioara. Edge computing in healthcare: Innovations, opportunities, and challenges. *Future internet*, 16(9):329, 2024.

[33] Sukhpal Singh Gill, Muhammed Golec, Jianmin Hu, Minxian Xu, Junhui Du, Huaming Wu, Guneet Kaur Walia, Subramaniam Subramanian Murugesan, Babar Ali, Mohit Kumar, et al. Edge ai: A taxonomy, systematic review and future directions. *Cluster Computing*, 28(1):1–53, 2025.

[34] Benjamin Recht, Rebecca Roelofs, Ludwig Schmidt, and Vaishaal Shankar. Do imagenet classifiers generalize to imagenet? In *International conference on machine learning*, pages 5389–5400. PMLR, 2019.

[35] Amin Naemi, Thomas Schmidt, Marjan Mansourvar, Mohammad Naghavi-Behzad, Ali Ebrahimi, and Uffe Kock Wiil. Machine learning techniques for mortality prediction in emergency departments: a systematic review. *BMJ open*, 11(11):e052663, 2021.

[36] Diana Barsasella, Karamo Bah, Pratik Mishra, Mohy Uddin, Eshita Dhar, Dewi Lena Suryani, Dedi Setiadi, Imas Masturoh, Ida Sugiarti, Jitendra Jonnagaddala, et al. A machine learning model to predict length of stay and mortality among diabetes and hypertension inpatients. *Medicina*, 58(11):1568, 2022.

[37] Guillem Hernández Guillamet, Ariadna Ning Morancho Pallaruelo, Laura Miró Mezquita, Ramón Miralles, Miquel Àngel Mas, María José Ulldemolins Papaseit, Oriol Estrada Cuxart, and Francesc López Seguí. Machine learning model for predicting mortality risk in patients with complex chronic conditions: Retrospective analysis. *Online Journal of Public Health Informatics*, 15:e52782, 2023.

[38] Kaiming He, Xiangyu Zhang, Shaoqing Ren, and Jian Sun. Deep residual learning for image recognition. In *Proceedings of the IEEE conference on computer vision and pattern recognition*, pages 770–778, 2016.

[39] Zachary Lipton, Yu-Xiang Wang, and Alexander Smola. Detecting and correcting for label shift with black box predictors. In *International conference on machine learning*, pages 3122–3130. PMLR, 2018.

[40] Jie Ren, Stanislav Fort, Jeremiah Liu, Abhijit Guha Roy, Shreyas Padhy, and Balaji Lakshminarayanan. A simple fix to mahalanobis distance for improving near-ood detection. *arXiv preprint arXiv:2106.09022*, 2021.

[41] Yaniv Ovadia, Emily Fertig, Jie Ren, Zachary Nado, David Sculley, Sebastian Nowozin, Joshua Dillon, Balaji Lakshminarayanan, and Jasper Snoek. Can you trust your model's uncertainty? evaluating predictive uncertainty under dataset shift. *Advances in neural information processing systems*, 32, 2019.

[42] David Lopez-Paz and Maxime Oquab. Revisiting classifier two-sample tests. *arXiv preprint arXiv:1610.06545*, 2016.

[43] Kuniaki Saito, Kohei Watanabe, Yoshitaka Ushiku, and Tatsuya Harada. Maximum classifier discrepancy for unsupervised domain adaptation. In *Proceedings of the IEEE conference on computer vision and pattern recognition*, pages 3723–3732, 2018.

[44] Tuan-Hung Vu, Himalaya Jain, Maxime Bucher, Matthieu Cord, and Patrick Pérez. Advent: Adversarial entropy minimization for domain adaptation in semantic segmentation. In *Proceedings of the IEEE/CVF conference on computer vision and pattern recognition*, pages 2517–2526, 2019.

[45] Dequan Wang, Evan Shelhamer, Shaoteng Liu, Bruno Olshausen, and Trevor Darrell. Tent: Fully test-time adaptation by entropy minimization. *arXiv preprint arXiv:2006.10726*, 2020.

[46] Xin Zhang and Ying-Cong Chen. Adaptive domain generalization via online disagreement minimization. *IEEE Transactions on Image Processing*, 32:4247–4258, 2023.

[47] Fei Ye and Adrian G Bors. Task-free continual learning via online discrepancy distance learning. *Advances in Neural Information Processing Systems*, 35:23675–23688, 2022.

[48] Jean Feng, Adarsh Subbaswamy, Alexej Gossmann, Harvineet Singh, Berkman Sahiner, Mi-Ok Kim, Gene Anthony Pennello, Nicholas Petrick, Romain Pirracchio, and Fan Xia. Designing monitoring strategies for deployed machine learning algorithms: navigating performativity through a causal lens. In Francesco Locatello and Vanessa Didelez, editors, *Proceedings of the Third Conference on Causal Learning and Reasoning*, volume 236 of *Proceedings of Machine Learning Research*, pages 587–608. PMLR, 01–03 Apr 2024.

[49] Jean Feng, Alexej Gossmann, Romain Pirracchio, Nicholas Petrick, Gene A Pennello, and Berkman Sahiner. Is this model reliable for everyone? testing for strong calibration. In Sanjoy Dasgupta, Stephan Mandt, and Yingzhen Li, editors, *Proceedings of The 27th International Conference on Artificial Intelligence and Statistics*, volume 238 of *Proceedings of Machine Learning Research*, pages 181–189. PMLR, 02–04 May 2024.

[50] Yiding Jiang, Vaishnavh Nagarajan, Christina Baek, and J Zico Kolter. Assessing generalization of sgd via disagreement. In *International Conference on Learning Representations*, 2022.

[51] Aleksandr Podkopaev and Aaditya Ramdas. Tracking the risk of a deployed model and detecting harmful distribution shifts. *arXiv preprint arXiv:2110.06177*, 2021.

[52] Tony Ginart, Martin Jinye Zhang, and James Zou. Mldemon: Deployment monitoring for machine learning systems. In *International conference on artificial intelligence and statistics*, pages 3962–3997. PMLR, 2022.

[53] Ziming Wang, Changwu Huang, and Xin Yao. Feature attribution explanation to detect harmful dataset shift. *2023 International Joint Conference on Neural Networks (IJCNN)*, pages 1–8, 2023.

[54] Vathy M Kamulete. Test for non-negligible adverse shifts. In *Uncertainty in Artificial Intelligence*, pages 959–968. PMLR, 2022.

[55] David Nigenda, Zohar Karnin, Muhammad Bilal Zafar, Raghu Ramesha, Alan Tan, Michele Donini, and Krishnaram Kenthapadi. Amazon sagemaker model monitor: A system for real-time insights into deployed machine learning models. In *Proceedings of the 28th ACM SIGKDD Conference on Knowledge Discovery and Data Mining*, pages 3671–3681, 2022.

[56] Kamyar Azizzadenesheli, Anqi Liu, Fanny Yang, and Animashree Anandkumar. Regularized learning for domain adaptation under label shifts. *arXiv preprint arXiv:1903.09734*, 2019.

[57] Shiyu Liang, Yixuan Li, and Rayadurgam Srikant. Enhancing the reliability of out-of-distribution image detection in neural networks. *arXiv preprint arXiv:1706.02690*, 2017.

[58] Jie Ren, Peter J Liu, Emily Fertig, Jasper Snoek, Ryan Poplin, Mark Depristo, Joshua Dillon, and Balaji Lakshminarayanan. Likelihood ratios for out-of-distribution detection. *Advances in neural information processing systems*, 32, 2019.

[59] Warren Morningstar, Cusuh Ham, Andrew Gallagher, Balaji Lakshminarayanan, Alex Alemi, and Joshua Dillon. Density of states estimation for out of distribution detection. In *International Conference on Artificial Intelligence and Statistics*, pages 3232–3240. PMLR, 2021.

[60] Shai Ben-David, John Blitzer, Koby Crammer, and Fernando Pereira. Analysis of representations for domain adaptation. *Advances in neural information processing systems*, 19, 2006.

[61] Shai Ben-David, John Blitzer, Koby Crammer, Alex Kulesza, Fernando Pereira, and Jennifer Wortman Vaughan. A theory of learning from different domains. *Machine learning*, 79:151–175, 2010.

[62] David Acuna, Guojun Zhang, Marc T Law, and Sanja Fidler. f-domain adversarial learning: Theory and algorithms. In *International Conference on Machine Learning*, pages 66–75. PMLR, 2021.

[63] Yaroslav Ganin, Evgeniya Ustinova, Hana Ajakan, Pascal Germain, Hugo Larochelle, François Laviolette, Mario March, and Victor Lempitsky. Domain-adversarial training of neural networks. *Journal of machine learning research*, 17(59):1–35, 2016.

[64] Shai Shalev-Shwartz and Shai Ben-David. *Understanding machine learning: From theory to algorithms*. Cambridge university press, 2014.

[65] Peter Bandi, Oscar Geessink, Quirine Manson, Marcory Van Dijk, Maschenka Balkenhol, Meyke Hermsen, Babak Ehteshami Bejnordi, Byungjae Lee, Kyunghyun Paeng, Aoxiao Zhong, et al. From detection of individual metastases to classification of lymph node status at the patient level: the camelyon17 challenge. *IEEE Transactions on Medical Imaging*, 2018.

[66] Djork-Arné Clevert, Thomas Unterthiner, and Sepp Hochreiter. Fast and accurate deep network learning by exponential linear units (elus). *arXiv preprint arXiv:1511.07289*, 2015.

[67] Sergey Ioffe and Christian Szegedy. Batch normalization: Accelerating deep network training by reducing internal covariate shift. In *International conference on machine learning*, pages 448–456. pmlr, 2015.

[68] Ilya Loshchilov and Frank Hutter. Decoupled weight decay regularization. *arXiv preprint arXiv:1711.05101*, 2017.

A Theoretical Setup and Analysis

A.1 Overview

In our experiments, we find that the D3M algorithm is effective in monitoring deteriorating changes in multi-class classification. As a proof of concept, we provide sample complexity analyses for the binary classification, where deteriorating shifts are shifts in the covariate distribution of data. We show that an ideal D3M algorithm can achieve strong TPR/FPR guarantees at desirable significance levels under these assumptions. We discuss the extent to which empirical observations from our experiments match with the insights revealed by this analysis.

A.2 Post-Deployment Deterioration (PDD) and Disagreement-based Post-Deployment Deterioration (D-PDD)

Consider a function class $\mathcal{H}$ of $h : \mathcal{X} \to \mathcal{Y} = \{0, 1\}$ in the binary classification setting. We use $g \in \mathcal{H}$ to denote the ground truth labeling function. We denote the marginal distribution w.r.t x as $\boldsymbol{P}_x(x)$ and the joint distribution with the labeling function in the subscript, that is, for a data distribution $\boldsymbol{P}_x$ over the domain $\mathcal{X}$ and any labeling function $g(x)$, we define the joint distribution as $\boldsymbol{P}_g = \boldsymbol{P}_g(x, y) = \boldsymbol{P}_x(x, g(x))$. For a $f \in \mathcal{H}$, define its generalization error with respect to $\boldsymbol{P}_g$ and its corresponding empirical counterpart with respect to a sample $\mathcal{D}^n = \{(x_i, y_i)\}_{i=1}^n \sim \boldsymbol{P}_g$ as:

$$\mathrm{err}(f; \boldsymbol{P}_g) \coloneqq \Pr_{(x,y)\sim \boldsymbol{P}_g} [f(x) \neq y], \qquad \widehat{\mathrm{err}}(f; \mathcal{D}^n) \coloneqq \widehat{\mathrm{err}}(f; \boldsymbol{P}_g) \coloneqq \frac{1}{n} \sum_{i=1}^{n} |f(x_i) - y_i|$$

Training and deployment distribution. We denote $\boldsymbol{P}_x$ as the training (marginal) distribution, and $\boldsymbol{Q}_x$ as the deployment distribution. We assume sampled batches of data are I.I.D. with respect to their underlying distribution $\boldsymbol{P}_x$ and/or $\boldsymbol{Q}_x$. We consider that $\boldsymbol{n}$ **labeled samples** from $\boldsymbol{P}_g$ are available before deployment, and $\boldsymbol{m}$ **unlabeled samples** from $\boldsymbol{Q}_x$ are collected during the deployment's input stream.

Disagreement. For any two functions f and h in $\mathcal{H}$, we say that they disagree on any point $x \in \mathcal{X}$ if $f(x) \neq h(x)$. Given the binary classification setting, we can write the disagreement rate of the function h with f on distribution $\boldsymbol{Q}_x$ in terms of error as $\mathrm{err}(h; \boldsymbol{Q}_f)$ or $\mathrm{err}(f; \boldsymbol{Q}_h)$.

Moving forward, $f \in \mathcal{H}$ will be understood to mean our base classifier obtained during training on $\mathcal{D}^n \sim \boldsymbol{P}_g$, while g is the ground truth on $\boldsymbol{P}_x$ and $h \in \mathcal{H}$ denotes auxiliary classifiers in the same hypothesis space, unless otherwise stated. Our goal is to study and monitor the following phenomenon:

Definition 1 (Post-deployment deterioration, PDD)**.** *Denote g and g' as ground truth labeling functions in the training and deployed distributions $\boldsymbol{P}_x$ and $\boldsymbol{Q}_x$ respectively. We say that PDD has occurred when:*

$$\mathrm{err}(f; \boldsymbol{Q}_{g'}) > \mathrm{err}(f; \boldsymbol{P}_g) \tag{1}$$

Intuitively, Eq. (1) suggests that PDD occurs when a model f experiences higher error during deployment than during its training. Due to the unsupervised nature of the deployment dataset, PDD monitoring is difficult for any arbitrary $g' \neq g$ as we cannot trivially compute empirical errors for the LHS. Though tools from the literature of OOD error estimation may be used, we propose to proxy via a related notion. Def. 2 introduces a new and practical concept—model disagreement-based PDD—equivalent to PDD under specific assumptions.

Definition 2 (Disagreement based PDD (D-PDD))**.** *We say that D-PDD has occurred when the following holds for some $\epsilon_f < 1$:*

$$\exists h \in \mathcal{H} \quad s.t. \quad \text{err}(h; \boldsymbol{P}_g) \leq \epsilon_f \text{ and } \text{err}(f; \boldsymbol{P}_g) \leq \epsilon_f \text{ and } \text{err}(h; \boldsymbol{Q}_f) > \text{err}(h; \boldsymbol{P}_f) \tag{2}$$

D-PDD in Def. 2 is defined as the situation where there exists an auxiliary model $h \in \mathcal{H}$ achieving equally good performance on $\boldsymbol{P}$ (with a small error ϵ_f) but exhibits strong disagreement with f in $\boldsymbol{Q}$. In this case, the distribution $\boldsymbol{Q}$ is further referred to as a **deteriorating shift**. In the following lemma, we demonstrate the conditions for the equivalence of PDD and D-PDD.

Lemma A.1 (Equivalence condition)**.** *Assume that the ground truth at training and deployment are identical, i.e. $g = g'$, and that $\text{TV}(\boldsymbol{P}, \boldsymbol{Q}) \leq \kappa$, we have that when $\text{err}(f, \boldsymbol{Q}_h) - \text{err}(f, \boldsymbol{P}_h) \geq 2(\kappa + \epsilon)$, i.e. the disagreement gap is large enough, D-PDD and PDD are equivalent.*

Proof. To show PDD $\implies$ D-PDD, assume $g = g'$, i.e. identical concepts during training and deployment. Assume our base classifier f is well-trained with $\text{err}(f, \boldsymbol{P}_g) = \epsilon$. We have that

$$\text{err}(f, \boldsymbol{Q}_g) > \text{err}(f, \boldsymbol{P}_g)$$

Let our candidate auxiliary function $h \in \mathcal{H}$ be given by $h = g$. Then, h satisfies all conditions for D-PDD.

We now show that D-PDD $\implies$ PDD. Assume that there is no concept shift, i.e. the ground truth distribution is identical, $g = g'$.

We transport the D-PDD condition $\exists h \in \mathcal{H}$ s.t. $\text{err}(f, \boldsymbol{Q}_h) > \text{err}(f, \boldsymbol{P}_h)$ to the general PDD condition $\text{err}(f, \boldsymbol{Q}_g) > \text{err}(f, \boldsymbol{P}_g)$ by leveraging the proximity of h to g on $\boldsymbol{P}$ and that the total variation between P and Q are constrained by κ.

We observe that for any $f, g, h \in \mathcal{H}$:

$$|\text{err}(f, \boldsymbol{P}_g) - \text{err}(f, \boldsymbol{P}_h)| < \epsilon$$

Indeed, this is true since:

$$\begin{aligned} |\text{err}(f, \boldsymbol{P}_g) - \text{err}(f, \boldsymbol{P}_h)| &= |\boldsymbol{P}(f \neq g) - \boldsymbol{P}(f \neq h)| \\ &= |\mathbb{E}_{\boldsymbol{P}}\left[\mathbb{1}\{f \neq g\} - \mathbb{1}\{f \neq h\}\right]| \\ &\leq \mathbb{E}_{\boldsymbol{P}}\left[|\mathbb{1}\{f \neq g\} - \mathbb{1}\{f \neq h\}|\right] \\ &\leq \mathbb{E}_{\boldsymbol{P}}\left[|\mathbb{1}\{g \neq h\}|\right] \\ &= \boldsymbol{P}(g \neq h) \leq \epsilon \end{aligned}$$

where we used Jensen's inequality, and that $|\mathbb{1}\{f \neq g\} + \mathbb{1}\{f \neq h\}| = |\mathbb{1}\{g \neq h\}|$.

Let $\text{TV}(\boldsymbol{P}, \boldsymbol{Q}) \leq \kappa$ for some $\kappa > 0$. We further observe that for any $f, g \in \mathcal{H}$:

$$\begin{aligned} |\text{err}(f, \boldsymbol{Q}_g) - \text{err}(f, \boldsymbol{P}_g)| &= |\boldsymbol{Q}(f \neq g) - \boldsymbol{P}(f \neq g)| \\ &\leq \sup_A |\boldsymbol{Q}(A) - \boldsymbol{P}(A)| = \kappa \end{aligned}$$

Putting our two observations together yields following decomposition:

$$\begin{aligned} |\text{err}(f, \boldsymbol{Q}_h) - \text{err}(f, \boldsymbol{Q}_g)| &\leq |\text{err}(f, \boldsymbol{Q}_h) - \text{err}(f, \boldsymbol{P}_h)| \\ &\quad + |\text{err}(f, \boldsymbol{P}_h) - \text{err}(f, \boldsymbol{P}_g)| + |\text{err}(f, \boldsymbol{P}_g) - \text{err}(f, \boldsymbol{Q}_g)| \\ &\leq 2\kappa + \epsilon \end{aligned}$$

For PDD to hold, $\text{err}(f, \boldsymbol{Q}_g)$ needs to be no less than $\text{err}(f, \boldsymbol{P}_h) + \epsilon$ and at most $2\kappa + \epsilon$ less than $\text{err}(f, \boldsymbol{Q}_h)$. Equating yields:

$$\text{err}(f, \boldsymbol{P}_h) + \epsilon \leq \text{err}(f, \boldsymbol{Q}_h) - 2\kappa - \epsilon$$

$$\implies \text{err}(f, \boldsymbol{Q}_h) - \text{err}(f, \boldsymbol{P}_h) \geq 2(\kappa + \epsilon)$$

prescribing the conditions for which D-PDD implies PDD.

□

Thus, if an algorithm monitors D-PDD, then under the assumptions of Lemma A.1, the algorithm also monitors post-deployment deterioration (PDD). In fact, D3M approximately monitors D-PDD. To see this, we show that an ideal version of D3M monitors D-PDD in the above subsection.

A.3 Idealized D3M and D-PDD Monitoring

Tracking D-PDD in finite samples as formulated requires training data during deployment, which runs counter to the set of desiderata we previously established. To circumvent this, we **decouple** the detection of D-PDD into two **Calibrate** and **Deploy** stages. The **Calibrate** stage finds a subset $\mathcal{H}_p \subset \mathcal{H}$ whose elements satisfy conditions on $\boldsymbol{P}_g$ in Def. 2 as well as approximates $\text{err}(h; \boldsymbol{P}_f)$, while the **Deploy** stage tracks the satisfaction of the last inequality. In this way, information from the training data is compressed into $\mathcal{H}_p$ and the approximation of $\text{err}(h; \boldsymbol{P}_f)$. Meanwhile, the approximation of the disagreement threshold $\text{err}(h, \boldsymbol{P}_f)$ for $h \in \mathcal{H}_p$ can be done via its empirical distribution Φ computed during the Calibrate phase. We thus present the idealized versions of the Calibrate and Deploy stages of D3M.

Algorithm 1 Idealized D3M: Calibrate

Require: $\mathcal{D}^n \sim \boldsymbol{P}_g$, f, ϵ, $\mathcal{H}$

Train a sub hypothesis space $\mathcal{H}_p := \{h \in \mathcal{H};\ \widehat{\text{err}}(h; \boldsymbol{P}_g) \leq \epsilon\}$
$\Phi \leftarrow []$
for $t \leftarrow 1, 2, \ldots, T$ **do**
  $\mathcal{D}^m \sim \boldsymbol{P}_f$
  $h \leftarrow \underset{h \in \mathcal{H}_p}{\text{argmax}}\ \widehat{\text{err}}(h; \mathcal{D}^m)$
  append $\widehat{\text{err}}(h; \mathcal{D}^m)$ to Φ
end for
return Φ, $\mathcal{H}_p$

1. Calibration in $\boldsymbol{P}$. Given in-distribution training data $\mathcal{D}^n$, a base model f trained on $\mathcal{D}^n$, an error tolerance ϵ, and the hypothesis class $\mathcal{H}$, we formulate the subset of $\mathcal{H}$ achieving the error tolerance, $\mathcal{H}_p = \{h \in \mathcal{H};\ \text{err}(h; \boldsymbol{P}_g) \leq \epsilon\}$. Then, the disagreement distribution Φ is trained: for T rounds, m samples pseudo-labeled by f ($\mathcal{D}^m$) is used to train auxiliary models h by maximizing disagreement between h and f under $\mathcal{H}_p$ on $\mathcal{D}^m$ to approximate $\text{dis}_P = \max_{h \in \mathcal{H}_p} \text{err}(h; \boldsymbol{P}_f)$. The empirical disagreement rate achieved by h is appended to Φ. Finally, the pre-training procedure returns Φ and $\mathcal{H}_p$.

Algorithm 2 Idealized D3M: Deploy

Require: $\mathcal{H}_p$, Φ, f, α

1: $\mathcal{D}^m \sim \boldsymbol{Q}_f$

2: $h \leftarrow \underset{h \in \mathcal{H}_p}{\operatorname{argmax}}\ \widehat{\operatorname{err}}(h; \mathcal{D}^m)$

3: **return** $\widehat{\operatorname{err}}(h; \mathcal{D}^m) >$ $(1-\alpha)$ quantile of Φ

2. Deploy in $\boldsymbol{Q}$. Given Φ and $\mathcal{H}_p$, we compute the one-sample approximation of the maximal disagreement with f on $\boldsymbol{Q}$: $\text{dis}_Q = \max_{h \in \mathcal{H}_p} \operatorname{err}(h; \boldsymbol{Q}_f)$. We say D-PDD happens when dis_Q lies in the top α quantile of Φ.

The idealized algorithms 1 and 2 together track D-PDD in finite samples. Indeed, a deployment on $\boldsymbol{Q}$ is flagged when the last inequality in Def. 2 is detected, while the imposition of the other inequalities are done via formulating the constrained hypothesis space $\mathcal{H}_p$ of hypotheses that already satisfy these inequalities and searching over it. Of note is that at deployment time, the original training set $\mathcal{D}^n$ is not required.

D3M approximates Idealized D3M. The primary implementation consideration in the Idealized D3M algorithms is the search over $\mathcal{H}_p$, which for large function classes cannot be done trivially. D3M "Bayesianly" approximates this search by turning the intractable optimization problem into a sampling problem. By drawing from our $(\text{VBLL}_\theta \circ \text{FE}_\theta)$ posterior, we are hoping to sample hypotheses that belong in $\mathcal{H}_p$ with high probability. When viewed this way, the correspondence between D3M and its idealized version above follows. The price of the increased efficiency from avoiding intractable searches over $\mathcal{H}_p$ is thus the sampling noise from D3M which may return hypotheses beyond the constraints of $\mathcal{H}_p$.

A.4 Provable Guarantees of Idealized D3M

We present theoretical guarantees for Idealized D3M (Algorithms 1 and 2), which we refer to as D3M for the remainder of this section. Recall that D3M is tracking a sufficient condition of D-PDD. We show that with enough samples, when there is non-deteriorating shift, the algorithm achieves low false positive rates with high probability. Then, we show that with enough samples, when there is deteriorating shift, the algorithm provably succeeds. Finally, we discuss pathological cases where monitoring fails irrespective of sample size.

A.4.1 Preliminary quantities

Definition 3 (Deployed classifier error)**.** *This quantifies the generalization error of the deployed base classifier f. This is measured on the distribution seen during training $\boldsymbol{P}_g$,*

$$\epsilon_f := \operatorname{err}(f; \boldsymbol{P}_g) \tag{3}$$

Indeed in Def. 2, we want the population error to be at most ϵ_f, which results in the constraint for the empirical error in the optimization problems of Algorithm 1 at most $\epsilon = \epsilon_f - \epsilon_0$, where ϵ_0 is a hyper-parameter to measure the gap between the empirical and population error.

We also define the VC dimensions of the hypothesis space $\mathcal{H}$ and the subset of interest $\mathcal{H}_p$ as:

$$\mathcal{H}_p := \{h \in \mathcal{H} : \operatorname{err}(h; \boldsymbol{P}_g) \leq \epsilon_f\}, \quad d_p := \text{VC}(\mathcal{H}_p), \quad d := \text{VC}(\mathcal{H})$$

Note that $d_p \leq d$. If the base classifier f is well-trained (ϵ_f is low), then d_p can be much smaller than d i.e., $d_p \ll d$.

Definition 4 (ϵ_p, ϵ_q maximum error in $\mathcal{H}_p$)**.** *The maximum error in $\mathcal{H}_p$ for both $\boldsymbol{P}$ and $\boldsymbol{Q}$ using pseudo-labels from f is defined as:*

$$\epsilon_p = \max_{h \in \mathcal{H}_p} \text{err}(h; \boldsymbol{P}_f), \quad \epsilon_q = \max_{h \in \mathcal{H}_p} \text{err}(h; \boldsymbol{Q}_f) \tag{4}$$

Note that empirical quantities of these are also the maximum empirical disagreement rates used in Algo. 1 and Algo. 2. Effectively, the algorithm detects $\epsilon_q - \epsilon_p > 0$ with finite samples.

Definition 5 (ξ quantifies D-PDD)**.** *We define ξ to quantify the degree of D-PDD. We adopt Def. 2 and define ξ as*

$$\xi := \max_{h \in \mathcal{H}_p} \{\text{err}(h; \boldsymbol{Q}_f) - \text{err}(h; \boldsymbol{P}_f)\} \tag{5}$$

Therefore, D3M detects whether $\xi > 0$. Furthermore, ξ is non-negative since $f \in \mathcal{H}_p$. Hence, in case of non-deteriorating shift, $\xi = 0$.

Note that $\xi \geq \epsilon_q - \epsilon_p$. It follows that $\epsilon_q - \epsilon_p > 0 \implies \xi > 0$, though the reverse implication is not necessarily true. Therefore Algo. 2, $(\epsilon_q - \epsilon_p > 0)$ is detecting a sufficient condition of D-PDD $(\xi > 0)$.

Next, we relate the amount of D-PDD, ξ, with the amount of distribution shift in the form of TV-distance between $\boldsymbol{P}_x$ and $\boldsymbol{Q}_x$. As seen in the Eq. 5, deterioration depends on the complexity of the function class and ϵ_f which affects the size of $\mathcal{H}_p$. We capture these factors by introducing a mixture distribution $\boldsymbol{U}$:

$$\boldsymbol{U} = \frac{1}{2}\left(\boldsymbol{P}_f + \boldsymbol{Q}_{1-f}\right) \tag{6}$$

Definition 6 (η error gap between $\mathcal{H}_p$ and Bayes optimal)**.** *For the distribution $\boldsymbol{U}$, the gap in error between the best classifier $h \in \mathcal{H}_p$ in the function class and the Bayes optimal classifier is η:*

$$\eta := \min_{h \in \mathcal{H}_p} \text{err}(h; \boldsymbol{U}) - \text{err}(f_{bayes}; \boldsymbol{U}) \tag{7}$$

Note that η depends on the shift and complexity of the function class. We relate various definitions introduced in this section as follows.

Proposition A.2 (D-PDD and TV distance)**.** *The relations between ξ (in Def. 5), η (in Def. 6), and ϵ_p, ϵ_q (in Def. 3 and 4) are as follows:*

$$\xi = \text{TV} - 2\eta \;\geq\; 0 \tag{8}$$

$$\xi \;\geq\; \epsilon_q - \epsilon_p \;\geq\; \xi - 2\epsilon_f \tag{9}$$

We denote the total variation distance between $\boldsymbol{P}_x$ and $\boldsymbol{Q}_x$ as TV. Intuitively, D-PDD is defined in such a way that after deployment, if we are uncertain of the performance of f, then the shift is deteriorating. In general, for simpler function classes such as linear models, by looking at one region of the domain ($\boldsymbol{P}_x$) it may be possible to be certain about the performance of another region ($\boldsymbol{Q}_x$), this is captured in Eq. 8. For very complex function classes, η can be low, hence $\xi > 0$ for most shifts. For simple function classes, η can be high, in which case ξ may not be positive and hence a non-deteriorating shift. This thus highlights a trade-off with selecting expressive functions to capture complex patterns in the data.

A.4.2 D3M algorithm in non-deteriorating shift

D3M aims to monitor and detect D-PDD in finite samples, which can inherently lead to false positives (FPR) when the shift is non-deteriorating. Therefore we set a tolerance factor α in Alg. 2 to account for the test's robustness. We show that for D3M, the FPR of the detection can be close to α for *any* shift in the data distribution. Furthermore, we show that the FPR can also be less than α in some cases. In the case of non deteriorating shift, by Def. 2, the following holds:

$$\forall h \in \mathcal{H}_p : \ \operatorname{err}(h; \boldsymbol{Q}_f) \leq \operatorname{err}(h; \boldsymbol{P}_f) \implies \epsilon_q \leq \epsilon_p \tag{10}$$

Note that D3M intuitively detects whether $\epsilon_q > \epsilon_p$. Since the above equation shows that $\epsilon_q \leq \epsilon_p$, given enough samples, the test will succeed. Recall that n is the number of samples given from $\boldsymbol{P}_g$ and m is the number of samples required from $\boldsymbol{Q}_x$. In the theorem below, the significance level α refers to the desired FPR.

Theorem A.3. *For $\gamma \leq \alpha$, when there is no deteriorating shift (no D-PDD) in Eq. 10, for a chosen significance level of α, the FPR of D3M is at most $\gamma + (1-\gamma)\ \mathcal{O}\left(\exp\left(-n\epsilon_0^2 + d\right)\right)$ if*

$$m \in \mathcal{O}\left(\left(\frac{1-\sqrt{\delta}}{\epsilon_p - \epsilon_q}\right)^2 \left(d_p + \ln\frac{1}{\gamma}\right)\right) \tag{11}$$

and $\epsilon_p - \epsilon_q > 0$, where $\delta = (d_p + \ln\frac{1}{\alpha})/(d_p + \ln\frac{1}{\gamma})$ and we define $\epsilon_0 \leq \epsilon_f - \widehat{\operatorname{err}}(h; \boldsymbol{P}_f)$.

In the case of non deteriorating shifts (specifically $\epsilon_p > \epsilon_q$) the FPR may be even less than α given that m and n are sufficiently large. The more samples from $\boldsymbol{Q}_x$ we have, the lesser the FPR in these cases. For any general case, by setting $\gamma = \alpha$ (i.e., $\delta = 1$) in the above theorem, we immediately have:

Corollary A.4. *For a chosen significance level α, the FPR of D3M (Alg. 2) is no more than $\alpha + (1-\alpha)\ \mathcal{O}\left(\exp\left(-n\epsilon_0^2 + d\right)\right)$.*

Practical insights. The corollary asserts the robustness of D3M against unnecessarily flagging non-deteriorating shifts. Independent of the number of deployment samples m, for any given significance level α, the FPR is only slightly worse, with the additive term decaying exponentially in the number of training samples. For many practical ML pipelines that by-and-large employ linear and forest models among others of manageable VC-dimension, having these guarantees means that a D3M audit likely won't negatively impact the continuity and quality of the model usage.

A.4.3 D3M algorithm in deteriorating shift

When deteriorating shift occurs:

$$\exists h \in \mathcal{H}_p : \operatorname{err}(h; \boldsymbol{Q}_f) > \operatorname{err}(h; \boldsymbol{P}_f) \tag{12}$$

However, this does not necessarily imply that $\epsilon_q > \epsilon_p$ which is ultimately the condition monitored by D3M. In the following, we break down the possible scenarios.

Regime 1. Deteriorating shift and $\epsilon_q > \epsilon_p$. In this case, Theorem A.5 demonstrates that the D3M algorithm detects deteriorating shift with provable high TPR. Here, the significance level α is understood to be 1 minus the desired TPR.

Theorem A.5. *For $\beta > 0$, when deteriorating shift occurs, for a chosen significance level of α, the TPR of D3M (Alg. 2) is at least $(1-\beta)\left(1-\mathcal{O}\left(\exp\left(-n\epsilon_0^2+d\right)\right)\right)$ if*

$$m \in \mathcal{O}\left(\left(\frac{1+\sqrt{\delta}}{\xi-2\epsilon_f}\right)^2\left(d_p+\ln\frac{1}{\beta}\right)\right) \tag{13}$$

and $\epsilon_q - \epsilon_p > 0$, where $\delta = (d_p + \ln\frac{1}{\alpha})/(d_p+\ln\frac{1}{\beta})$, and $\epsilon_0 \leq \epsilon_f - \widehat{\text{err}}(h; \boldsymbol{P}_f)$.

Notably, ξ in the denominator indicates that as the shift becomes more deteriorating, D3M requires fewer samples m to detect, evidencing its effectiveness. Further, having a high-quality base classifier f with low ϵ_f is better for detection: this is seen through in Eq. 9 where low ϵ_f makes the monitoring more faithful at a lower sample complexity m. Another remark is that m depends on d_p which can be much less than d with n being dependent on the latter. The test, thus, can work for a m significantly smaller than n. The dependency on n is due to the requirement of satisfaction of the first condition in Def. 2. In the constrained optimization problems in Algo. 1, the constraint is satisfied but the population constraint will be satisfied either for a larger ϵ_0 or for sufficiently large n as seen in the above theorem.

Regime 2. (Possible tradeoff) -Deteriorating shift but $\epsilon_q \leq \epsilon_p$. In this case, Theorem A.6 demonstrates that either the false negative or false positive rates (FNR, FPR) should be high. The illustration in Fig. 4 exemplifies this failure mode, and how a low ϵ_f can help alleviate it.

Theorem A.6. *When deteriorating shift occurs and $\epsilon_q \leq \epsilon_p$, for a chosen significance level of α, the TPR of Alg. 2 is $\mathcal{O}(\alpha)$.*

If α is low, then by Theorem A.6 we have that the FNR is high. On the other hand, if α is high, then by Corollary A.4 we have that the FPR can be very high, thereby trading off the significance level of D3M to reduce FNR but loosening guarantees on FPRs.

A.4.4 Solutions for FNR/FPR tradeoff

This part provides a possible failure scenario illustrated in Fig. 4. Notably, we will highlight a badly trained base classifier f in the possible failure scenario (Fig. 4 (a)), if f is trained with lower ϵ_f, can move to the scenarios (Fig. 4 (b) and (c)) where the D3M algorithm can succeed.

In Fig. 4 (a), if f is not well-trained, we will encounter a failure scenario. The disagreement of h_1 with f on $\boldsymbol{Q}_x$ is larger than that of $\boldsymbol{P}_x$, evidencing D-PDD. However, note that h_2 can maximize ϵ_p more than any function (in $\mathcal{H}_p$) can maximize ϵ_q, which implies $\epsilon_p > \epsilon_q$. If f is better trained in Fig. 4 (b), for all functions in $\mathcal{H}_p$ (curves between h_1 and h_2) disagreement with f on $\boldsymbol{P}_x$ is not less than that of $\boldsymbol{Q}_x$. Hence there is no deteriorating shift and D3M algorithm could provably address this. Alternatively, if f is trained well and is closest to the ground truth Fig. 4 (c) the disagreement of h_2 with f on $\boldsymbol{Q}_x$ is more than that of $\boldsymbol{P}_x$. Also, note that $\epsilon_p = 0$ since there is no function that can have any error on $\boldsymbol{P}_f$. However, h_2 can be the classifier to get non-zero ϵ_q which gives $\epsilon_q > \epsilon_p$. Hence (c) recovers the Regime 1 and is solvable.

Practical implications. Training base classifiers with strong in-distribution generalization performance helps in reducing the likelihood of falling into **Regime 2**. Then, Theorem A.6 guarantees that with high probability, the desired TPR of D3M can be achieved modulo an exponentially decaying factor in the number of training samples. In this way, D3M is robust in monitoring deteriorating shifts with provable TPR guarantees, satisfying the robustness desiderata for PDD monitoring.

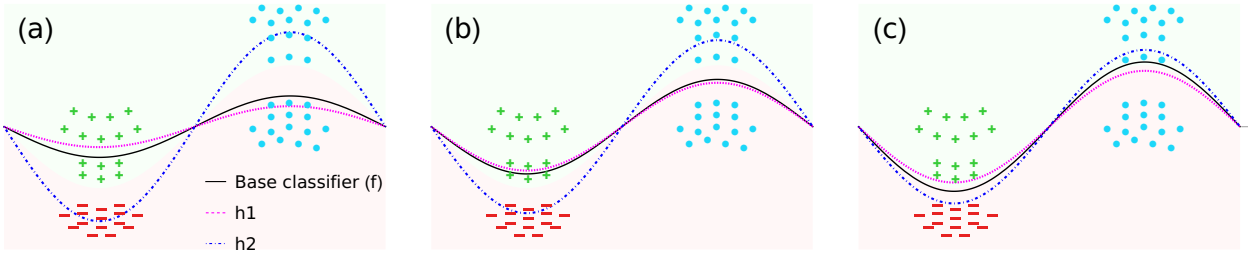

Figure 4: Illustration of the FNR/FPR tradeoff and its remedy. The background color indicates the fixed ground truth. Positive and Negative points are from $\boldsymbol{P}_g$ (labeled) and the unlabeled points are from $\boldsymbol{Q}_x$. The solid black curve represents the deployed base classifier f. The dotted Pink (h_1) and Blue (h_2) curves represent the envelope boundary for $\mathcal{H}_p$ i.e., all the functions passing between these two curves are contained in $\mathcal{H}_p$. (a) Failure scenario (i.e, Regime 2) where D3M algorithm fails. (b) No deteriorating shift scenario. (c) Deteriorating shift and the D3M algorithm succeeds. In summery, a decreasing on ϵ_f could move the failure scenario to the solvable scenarios (a) or (b).

A.5 Proofs

Lemma A.7. *For any $\gamma > 0$, $\mu > \epsilon_q$, we have $\widehat{\text{err}}(h; \boldsymbol{Q}_f) \leq \mu$ for all $h \in \mathcal{H}_p$ with probability at least $1 - \gamma$ if*

$$m \in \mathcal{O}\left(\frac{d_p + \ln \frac{1}{\gamma}}{(\mu - \epsilon_q)^2}\right) \tag{14}$$

Proof. We use the generalization bound for agnostic learning in [64].

$$ce^{d_p} e^{-\epsilon^2 m} \geq \Pr_{X,Y \sim \boldsymbol{Q}_{1-f}^m} [\exists h \in \mathcal{H}_p : \text{err}(h; \boldsymbol{Q}_{1-f}) - \widehat{\text{err}}(h; \boldsymbol{Q}_{1-f}) \geq \epsilon] \tag{15}$$

$$= \Pr_{X,Y \sim \boldsymbol{Q}_{1-f}^m} [\exists h \in \mathcal{H}_p : \widehat{\text{err}}(h; \boldsymbol{Q}_f) \geq \text{err}(h; \boldsymbol{Q}_f) + \epsilon] \tag{16}$$

$$\geq \Pr_{X,Y \sim \boldsymbol{Q}_{1-f}^m} [\exists h \in \mathcal{H}_p : \widehat{\text{err}}(h; \boldsymbol{Q}_f) \geq \epsilon_q + \epsilon] \tag{17}$$

Choose $\epsilon = \mu - \epsilon_q$ for any $\mu > \epsilon_q$. Now,

$$ce^{d_p} e^{-\epsilon^2 m} \leq \gamma \tag{18}$$

$$m \in \mathcal{O}\left(\frac{d_p + \ln \frac{1}{\gamma}}{(\mu - \epsilon_q)^2}\right) \tag{19}$$

□

Lemma A.8. *For any $h \in \mathcal{H}$, if the $\widehat{\text{err}}(h; \boldsymbol{P}_f) \leq \epsilon_f - \epsilon_0$ then with probability at least $1 - \mathcal{O}\left(\exp\left(-n\epsilon_0^2 + d\right)\right)$, h will be in $\mathcal{H}_p$*

Proof. We use the generalization bound for agnostic learning in [64].

$$ce^d e^{-\epsilon^2 n} \geq \Pr_{X,Y\sim \boldsymbol{P}_g^n}\left[\exists h \in \mathcal{H} : \text{err}(h; \boldsymbol{P}_g) - \widehat{\text{err}}(h; \boldsymbol{P}_g) \geq \epsilon\right] \tag{20}$$

$$= \Pr_{X,Y\sim \boldsymbol{P}_g^n}\left[\exists h \in \mathcal{H} : \text{err}(h; \boldsymbol{P}_g) \geq \widehat{\text{err}}(h; \boldsymbol{P}_g) + \epsilon\right] \tag{21}$$

$$\geq \Pr_{X,Y\sim \boldsymbol{P}_g^n}\left[\exists h \in \mathcal{H} : \text{err}(h; \boldsymbol{P}_g) \geq \epsilon_f - \epsilon_0 + \epsilon\right] \tag{22}$$

Choose $\epsilon = \epsilon_0$ to get

$$\Pr_{X,Y\sim \boldsymbol{P}_g^n}\left[\exists h \in \mathcal{H} : \text{err}(h; \boldsymbol{P}_g) \geq \epsilon_f\right] \leq ce^d e^{-\epsilon^2 n} \tag{23}$$

□

Theorem A.9. *For $\gamma \leq \alpha$, when there is no deteriorating shift, for a chosen significance level of α, the FPR of Algo. 2 is at most $\gamma + (1-\gamma)\ \mathcal{O}\left(\exp\left(-n\epsilon_0^2 + d\right)\right)$ if*

$$m \in \mathcal{O}\left(\left(\frac{1-\sqrt{\delta}}{\epsilon_p - \epsilon_q}\right)^2 \left(d_p + \ln\frac{1}{\gamma}\right)\right) \tag{24}$$

and $\epsilon_p - \epsilon_q > 0$, where $\delta = \frac{d_p + \ln\frac{1}{\alpha}}{d_p + \ln\frac{1}{\gamma}}$

Proof. We show that in the case of no deteriorating shift (which implies $\epsilon_p \geq \epsilon_q$) the false positive rate cannot be more than α and also having more samples from $\boldsymbol{Q}_x$ will decrease the false positive rate if $\epsilon_p > \epsilon_q$.

We assume that during pre-training phase, while populating Φ we discard disagreement from $h \notin \mathcal{H}_p$ i.e., not satisfying the constraint $\text{err}(h; \boldsymbol{P}_f) \leq \epsilon_f$. We cannot do the same during the detection phase since the detection phase is time-sensitive. Due to this, we have to account for $h \notin \mathcal{H}_p$ in the FPR calculation.

Now, FPR can be written and bounded as follows. Let μ be the disagreement at $1-\alpha$ percentile of Φ

$$\text{FPR} = \Pr\left[\widehat{\text{err}}(h; \boldsymbol{Q}_f) \geq \mu\right] \tag{25}$$

$$= \Pr\left[\{\{h \notin \mathcal{H}_p\} \wedge \{\widehat{\text{err}}(h; \boldsymbol{Q}_f) \geq \mu\}\} \vee \{\{h \in \mathcal{H}_p\} \wedge \{\widehat{\text{err}}(h; \boldsymbol{Q}_f) \geq \mu\}\}\right] \tag{26}$$

$$\leq \Pr\left[\{h \notin \mathcal{H}_p\} \vee \{\{h \in \mathcal{H}_p\} \wedge \{\widehat{\text{err}}(h; \boldsymbol{Q}_f) \geq \mu\}\}\right] \tag{27}$$

$$\leq \Pr\left[h \notin \mathcal{H}_p\right] + \Pr\left[\{\widehat{\text{err}}(h; \boldsymbol{Q}_f) \geq \mu\} \mid \{h \in \mathcal{H}_p\}\right] \Pr\left[h \in \mathcal{H}_p\right] \tag{28}$$

$$= \gamma + (1-\gamma)\Pr\left[h \notin \mathcal{H}_p\right] \tag{29}$$

$$\text{FPR} \leq \gamma + (1-\gamma)\ \mathcal{O}\left(\exp\left(-n\epsilon_0^2 + d\right)\right) \tag{30}$$

where last equation comes from A.8 and $\gamma := \Pr\left[\{\widehat{\text{err}}(h; \boldsymbol{Q}_f) \geq \mu\} \mid \{h \in \mathcal{H}_p\}\right]$

Now, we derive sample complexity m in terms of γ. Using A.7 on $\boldsymbol{P}$ with $1-\alpha$ probability we get

$$m \in \mathcal{O}\left(\frac{d_p + \ln\frac{1}{\alpha}}{(\mu - \epsilon_p)^2}\right) \tag{31}$$

We use $\mu \in \Omega\left(\epsilon_p + \sqrt{\frac{d_p + \ln\frac{1}{\alpha}}{m}}\right)$ from above while using A.7 on $\boldsymbol{Q}$ with $1-\gamma$ probability to get

$$m \in \mathcal{O}\left(\left(\frac{1 - \sqrt{\frac{d_p+\ln\frac{1}{\alpha}}{d_p+\ln\frac{1}{\gamma}}}}{(\epsilon_p - \epsilon_q)}\right)^2 \left(d_p + \ln\frac{1}{\gamma}\right)\right) \quad \text{for } \gamma < \alpha \tag{32}$$

Note that since the chosen μ was greater than ϵ_p and we are dealing with the case $\epsilon_p > \epsilon_q$, we get that the chosen μ is greater than ϵ_q. Thus the requirement of μ is satisfied for A.7 while using for $\boldsymbol{Q}$. □

This theorem shows that when there are non deteriorating shifts (specifically $\epsilon_p > \epsilon_q$) FPR may be even less than α, given m and n is sufficiently large. The more samples from $\boldsymbol{Q}_x$ we have the lesser the FPR in these cases. For any general case, by setting $\gamma = \alpha$ (i.e., $\delta = 1$) in the above theorem, we obtain the following:

Corollary A.10. *For a chosen significance level α, the FPR of the D3M algorithm is no more than $\alpha + (1-\alpha)\ \mathcal{O}\left(\exp\left(-n\epsilon_0^2 + d\right)\right)$.*

Note that this statement is independent of m and the distribution shift. If n is sufficiently large, the exponential term is small. This is often the case when the base classifier error ϵ_f is small, which is an indicator that a large number of samples (n) were available from $\boldsymbol{P}_g$. Ignoring non deteriorating shift (and $\boldsymbol{Q}_x \neq \boldsymbol{P}_x$) cases while calculating Φ in Algo. 2 does not adversely affect the FPR of the test.

Lemma A.11. *For any $\beta > 0, \mu < \epsilon_q$, there exists an $h \in \mathcal{H}_p$ such that $\widehat{\text{err}}(h; \boldsymbol{Q}_f) \geq \mu$ with probability at least $1-\beta$ if*

$$m \geq \mathcal{O}\left(\frac{d_q + \ln\frac{1}{\beta}}{(\epsilon_q - \mu)^2}\right) \tag{33}$$

Proof. We use the generalization bound for agnostic learning case [64].

$$ce^{d_p}e^{-\epsilon^2 m} \geq \Pr_{X,Y\sim\boldsymbol{Q}_{1-f}^m}[\exists h \in \mathcal{H}_p : \widehat{\text{err}}(h; \boldsymbol{Q}_{1-f}) - \text{err}(h; \boldsymbol{Q}_{1-f}) \geq \epsilon] \tag{34}$$

$$= \Pr_{X,Y\sim\boldsymbol{Q}_{1-f}^m}[\exists h \in \mathcal{H}_p : \widehat{\text{err}}(h; \boldsymbol{Q}_f) \leq \text{err}(h; \boldsymbol{Q}_f) - \epsilon] \tag{35}$$

$$\overset{(a)}{=} \Pr_{X,Y\sim\boldsymbol{Q}_{1-f}^m}[\forall h \in \mathcal{H}_p : \widehat{\text{err}}(h; \boldsymbol{Q}_f) \leq \epsilon_q - \epsilon] \tag{36}$$

where (a) follows from Def. 4
Choose $\epsilon = \epsilon_q - \mu$ for any $\mu < \epsilon_q$

$$ce^{d_q}e^{-\epsilon^2 m} \leq \beta \tag{37}$$

$$m \geq \mathcal{O}\left(\frac{d_q + \ln\frac{1}{\beta}}{(\epsilon_q - \mu)^2}\right) \tag{38}$$

□

Proposition A.12 (D-PDD and TV distance)**.** *The relations between ξ (in Def. 5), η (in Def. 6), and ϵ_p, ϵ_q (in Def. 3 and 4) are as follows:*

$$\xi = \mathrm{TV} - 2\eta \;\geq\; 0 \tag{39}$$

$$\xi \;\geq\; \epsilon_q - \epsilon_p \;\geq\; \xi - 2\epsilon_f \tag{40}$$

Proof. Recall the definition of $\boldsymbol{U}$ from 6. We first derive the Bayes error in terms of TV distance. Let

$$A = \{x \in \mathcal{X} \mid \boldsymbol{Q}_x(x) \leq \boldsymbol{P}_x(x)\} \tag{41}$$

$$A' = \{x \in \mathcal{X} \mid \boldsymbol{Q}_x(x) > \boldsymbol{P}_x(x)\} \tag{42}$$

The TV distance is equal to half of the L_1 distance. Note that $\boldsymbol{P}_x(A) + \boldsymbol{P}_x(A') = 1$ and similarly for $\boldsymbol{Q}_x$. [2]

$$\mathrm{TV}(\boldsymbol{P}_x, \boldsymbol{Q}_x) = \frac{1}{2}\left(\boldsymbol{P}_x(A) - \boldsymbol{Q}_x(A) + \boldsymbol{Q}_x(A') - \boldsymbol{P}_x(A')\right) \tag{43}$$

$$= 1 - \boldsymbol{P}_x(A') - \boldsymbol{Q}_x(A) \tag{44}$$

Now, we use the definition of $\boldsymbol{U}$ and the above TV relation to get the following

$$\mathrm{err}\left(f_{\mathrm{bayes}}; \boldsymbol{U}\right) = \frac{1}{2}\left(\mathrm{err}\left(f_{\mathrm{bayes}}; \boldsymbol{P}_f\right) + \mathrm{err}\left(f_{\mathrm{bayes}}; \boldsymbol{Q}_{1-f}\right)\right) = \frac{1}{2}\left(\boldsymbol{Q}_x(A) + \boldsymbol{P}_x(A')\right) \tag{45}$$

$$= \frac{1}{2}\left(1 - \mathrm{TV}(\boldsymbol{P}_x, \boldsymbol{Q}_x)\right) \tag{46}$$

Next, with the above result and η in Eq. 6 we derive Eq. 8

$$\eta + \mathrm{err}(f_{\mathrm{bayes}}; \boldsymbol{U}) = \min_{h \in \mathcal{H}_p} \mathrm{err}(h; \boldsymbol{U}) = \frac{1}{2} \min_{h \in \mathcal{H}_p} \left(\mathrm{err}(h; \boldsymbol{P}_f) + \mathrm{err}(h; \boldsymbol{Q}_{1-f})\right) \tag{47}$$

$$2\eta + 1 - \mathrm{TV} = \min_{h \in \mathcal{H}_p} \left(\mathrm{err}(h; \boldsymbol{P}_f) + \mathrm{err}(h; \boldsymbol{Q}_{1-f})\right) \geq \min_{h \in \mathcal{H}_p} \mathrm{err}(h; \boldsymbol{Q}_{1-f}) \tag{48}$$

$$2\eta + 1 - \mathrm{TV} = \min_{h \in \mathcal{H}_p} \left(\mathrm{err}(h; \boldsymbol{P}_f) - \mathrm{err}(h; \boldsymbol{Q}_f)\right) + 1 \tag{49}$$

$$2\eta - \mathrm{TV} = \min_{h \in \mathcal{H}_p} -\left(\mathrm{err}(h; \boldsymbol{Q}_f) - \mathrm{err}(h; \boldsymbol{P}_f)\right) \tag{50}$$

$$\mathrm{TV} - 2\eta = \max_{h \in \mathcal{H}_p} \left(\mathrm{err}(h; \boldsymbol{Q}_f) - \mathrm{err}(h; \boldsymbol{P}_f)\right) = \xi \tag{51}$$

For Eq. 9, we use Eq. 48 and the above result to get the following

$$\epsilon_q = \max_{h \in \mathcal{H}_p} \mathrm{err}(h; \boldsymbol{Q}_f) = 1 - \min_{h \in \mathcal{H}_p} \mathrm{err}(h; \boldsymbol{Q}_{1-f}) \geq \mathrm{TV} - 2\eta = \xi \tag{52}$$

We can write an inequality for errors similar to triangle inequality as follows

$$\mathrm{err}(h; \boldsymbol{P}_f) \leq \mathrm{err}(h; \boldsymbol{P}_g) + \mathrm{err}(g; \boldsymbol{P}_f) \tag{53}$$

$$= \mathrm{err}(h; \boldsymbol{P}_g) + \mathrm{err}(f; \boldsymbol{P}_g) = \mathrm{err}(h; \boldsymbol{P}_g) + \epsilon_f \tag{54}$$

$$\epsilon_p = \max_{h \in \mathcal{H}_p} \mathrm{err}(h; \boldsymbol{P}_f) \leq \max_{h \in \mathcal{H}_p} \mathrm{err}(h; \boldsymbol{P}_g) + \epsilon_f = 2\epsilon_f \tag{55}$$

The last equality follows from the definition of $\mathcal{H}_p$. Thus we get

$$\epsilon_q - \epsilon_p \geq \xi - 2\epsilon_f \tag{56}$$

By definition it follows that $\xi \geq \epsilon_q - \epsilon_p$ □

[2] With some abuse of notation, we use the same notation for both pdf and probability measure.

Proposition A.13. *For $\beta > 0$, when the deteriorating shift occurs, for a chosen significance level of α, the TPR of Algo. 2 is at least $(1-\beta)\left(1-\mathcal{O}\left(\exp\left(-n\epsilon_0^2+d\right)\right)\right)$ if*

$$m \in \mathcal{O}\left(\left(\frac{1+\sqrt{\delta}}{\xi-2\epsilon_f}\right)^2\left(d_p+\ln\frac{1}{\beta}\right)\right) \tag{57}$$

and $\epsilon_q - \epsilon_p > 0$, where $\delta = \frac{d_p+\ln\frac{1}{\alpha}}{d_p+\ln\frac{1}{\beta}}$

Proof. Similar to the proof of Theorem. A.3, we derive the statistical power (TPR) of the test as follows. Let μ be the disagreement at $1-\alpha$ percentile of Φ

$$\begin{aligned}
\text{TPR} &= 1 - \Pr\left[\widehat{\text{err}}(h;\boldsymbol{Q}_f) \le \mu\right] && (58)\\
&= 1 - \Pr\left[\{\{h \notin \mathcal{H}_p\} \wedge \{\widehat{\text{err}}(h;\boldsymbol{Q}_f) \le \mu\}\} \vee \{\{h \in \mathcal{H}_p\} \wedge \{\widehat{\text{err}}(h;\boldsymbol{Q}_f) \le \mu\}\}\right] && (59)\\
&\ge 1 - \Pr\left[\{h \notin \mathcal{H}_p\} \vee \{\{h \in \mathcal{H}_p\} \wedge \{\widehat{\text{err}}(h;\boldsymbol{Q}_f) \le \mu\}\}\right] && (60)\\
&\ge 1 - \Pr\left[h \notin \mathcal{H}_p\right] - \Pr\left[\{\widehat{\text{err}}(h;\boldsymbol{Q}_f) \le \mu\} \mid \{h \in \mathcal{H}_p\}\right]\Pr\left[h \in \mathcal{H}_p\right] && (61)\\
&= (1-\beta)\Pr\left[h \in \mathcal{H}_p\right] && (62)\\
\text{TPR} &\in (1-\beta)\left(1-\mathcal{O}\left(\exp\left(-n\epsilon_0^2+d\right)\right)\right) && (63)
\end{aligned}$$

where last equation comes from A.8 and $\beta := \Pr\left[\{\widehat{\text{err}}(h;\boldsymbol{Q}_f) \le \mu\} \mid \{h \in \mathcal{H}_p\}\right]$

Next, we derive the sample complexity m in terms of β. We show that there exists a μ^* such that both A.7 (for $\boldsymbol{P}$ and α) and A.11 (for $\boldsymbol{Q}$ and β) hold.

$$\epsilon_p < \mu < \epsilon_q \tag{64}$$

This implies some μ exists if $\epsilon_q - \epsilon_p > 0$
We find optimal μ^* such that the maximum of m in Eq. 14 and Eq. 33 is minimized.

$$\left(\frac{\mu-\epsilon_p}{\epsilon_q-\mu}\right)^2 = \frac{d_p+\ln\frac{1}{\alpha}}{d_p+\ln\frac{1}{\beta}} := \delta \tag{65}$$

$$\mu^* = \frac{\epsilon_p+\sqrt{\delta}\epsilon_q}{1+\sqrt{\delta}} \tag{66}$$

Plugging this μ^* in Eq. 33 gives

$$m \in \mathcal{O}\left(\frac{d+\ln\frac{1}{\beta}}{(\epsilon_q-\epsilon_p)^2}\left(1+\sqrt{\frac{d+\ln\frac{1}{\alpha}}{d+\ln\frac{1}{\beta}}}\right)^2\right) \tag{67}$$

Use Eq. 9 to get the result. □

ξ in the denominator indicates that as the shift becomes more deteriorating, it is easier (fewer samples m) to monitor, indicating the effectiveness of the D3M algorithm. Also, having a high-quality base classifier (low ϵ_f) is better for D3M which was also seen in Eq. 9 where low ϵ_f makes the algorithm more faithful. Note that m depends on d_p which can be much less than d which n depends on, suggesting that monitoring may be effective in few-shot settings. The dependence on n is due to the requirement of satisfaction of condition 1 in Def. 2. In the optimization problems in Algo. 1, the empirical constraint is satisfied but the population constraint will be satisfied either for larger ϵ_0 or for sufficiently large n as seen in the theorem.

Next, we move to the regime where deteriorating shift occurs but $\epsilon_q - \epsilon_q \le 0$. As a negative result, the following theorem states that in such cases the statistical power of the test is low.

Theorem A.14. *When deteriorating shift occurs and $\epsilon_q \leq \epsilon_p$, for a chosen significance level of α, the statistical power of the test in Alg. 2 is $\mathcal{O}(\alpha)$.*

Proof. From the proof of Theorem. A.5 we have

$$\text{TPR} \geq (1-\beta)\left(1-\mathcal{O}\left(\exp\left(-n\epsilon_0^2+d\right)\right)\right) \tag{68}$$

$$\beta := \Pr\left[\{\widehat{\text{err}}(h;\boldsymbol{Q}_f) \leq \mu\} \,|\, \{h \in \mathcal{H}_p\}\right] \tag{69}$$

Using A.7 on $\boldsymbol{P}$ and α we get

$$\alpha \in \mathcal{O}(\exp\left(-n(\mu-\epsilon_p)^2+d_p\right)) \tag{70}$$

Using A.7 on $\boldsymbol{Q}$ we get

$$\Pr\left(\{\widehat{\text{err}}(h;\boldsymbol{Q}_f) \geq \mu\} \,|\, \{h \in \mathcal{H}_p\}\right) \in \mathcal{O}\left(\exp\left(-n(\mu-\epsilon_q)^2+d_p\right)\right) \tag{71}$$

$$1-\beta \in \mathcal{O}\left(\exp\left(-n(\mu-\epsilon_q)^2+d_p\right)\right) \tag{72}$$

$$1-\beta \in \mathcal{O}\left(\alpha\right) \tag{73}$$

The last equation follows since we are dealing with the case where $\epsilon_p \geq \epsilon_q$. Thus, the TPR is $\mathcal{O}(\alpha)$ irrespective of the magnitude of n, as desired. □

B Experimental Setup and Additional Details

B.1 Baselines Details

We compare D3M against several other methods from the literature that either detect distribution changes or **can be converted into a PDD monitoring protocol**. Let $\boldsymbol{X} = \{\boldsymbol{x}^{(i)}\}_{i=1}^{n}$ from $\boldsymbol{P}_x$ and $\boldsymbol{Y} = \{\boldsymbol{y}^{(i)}\}_{i=1}^{m}$ from $\boldsymbol{Q}_x$ be given. These algorithms seek to accept or reject the hypothesis that $\boldsymbol{P}_x = \boldsymbol{Q}_x$ in distribution.

1. Deep Kernel MMD (MMD-D, [13]) The algorithm first learns a deep kernel by optimizing a criterion which yields the most powerful hypothesis test. With this learned kernel, permutation tests are run multiple times in order to determine a true positive rate for the algorithm. We interface the authors' original source code with our repository and recycle their training procedures. Theirs can be found at https://github.com/fengliu90/DK-for-TST.

2. H-Divergence (H-Div, [14]) The algorithm fits Gaussian kernel density estimates for $\boldsymbol{P}_x$, $\boldsymbol{Q}_x$, and their uniform mixture $(\boldsymbol{P}_x + \boldsymbol{Q}_x)/2$. Then, permutation tests are performed using the test statistic $H_\ell((\boldsymbol{P}_x + \boldsymbol{Q}_x)/2) - \min\{H_\ell(\boldsymbol{Q}_x), H_\ell(\boldsymbol{P}_x)\}$ where H_ℓ is the H-entropy with $\ell(x, a)$ the negative log likelihood of x under distribution a estimated by the Gaussian kernel density, in order to determine a true positive rate for the algorithm. This test statistic is an empirical estimate of the H-Min divergence. The choice of the particular H-divergence is a hyperparameter and is problem dependent, as well as the choice for how to generatively model the data distributions. The original paper further experimented with fitting Gaussian distributions as well as variational autoencoders (VAEs), both of which are not explored here. We interface the authors' original source code with our repository. Theirs can be found at https://github.com/a7b23/H-Divergence/tree/main.

3. f-Divergences (KL-Div for KL-Divergence, JS-Div for Jensen-Shannon Divergence, [62]) f-divergence generalizes several notions of distances between probability distributions commonly used in machine learning. In this paper, we convert the Kullback-Leibler (KL) and the Jensen-Shannon (JS) divergences, particular cases of f-divergences, into permutation tests. More specifically, we first fit Gaussians on samples coming from $\boldsymbol{P}_x$ and $\boldsymbol{Q}_x$ using maximum likelihood. In the case of KL-divergence, the empirical KL-divergence is computed between the fitted Gaussians whereas for the JS-divergence, we fit an additional Gaussian on the mixture distribution $\boldsymbol{M}$ and leverage the identity:

$$\mathrm{JS}(\boldsymbol{P}_x||\boldsymbol{Q}_x) = \frac{1}{2}(\mathrm{KL}(\boldsymbol{P}_x||\boldsymbol{M}) + \mathrm{KL}(\boldsymbol{Q}_x||\boldsymbol{M}))$$

   We run permutation tests by permuting the samples in the union $(X \sim \boldsymbol{P}_x^n) \cup (Y \sim \boldsymbol{Q}_x^m)$. It is worth noting that as with H-divergence, more elaborate generative models could be fitted onto samples X and Y, which we do not explore in this work.

4. Black Box Shift Detection (BBSD, [39]) involves estimating the changes in the distribution of target labels $p(y)$ between training and test data while assuming that the conditional distribution of features given labels $p(x|y)$ remains constant. This is achieved by using a black box model's confusion matrix to identify discrepancies in the marginal label probabilities between the training and test distributions, allowing detection and correction of the shift. We borrow the experimental setup directly from [1].

5. Relative Mahalanobis Distance (RMD, Rel-MH, Rel. Mahalanobis, [40]) RMD modifies the traditional Mahalanobis Distance (MD) for out-of-distribution (OOD) detection by accounting for the influence of non-discriminative features. It subtracts the MD of a test sample to a background class-independent Gaussian from the MD to each class-specific Gaussian, effectively isolating discriminative features and improving OOD detection, especially for near-OOD tasks. We test for shift by performing a KS test directly on the distribution of the RMD confidence scored computed on $\boldsymbol{Q}_x$ and $\boldsymbol{P}_x$.

6. Classifier two-sample test (CTST, C2ST, a.k.a. Domain Classifier, DC, [42]) Following the procedure presribed by the original work, a binary domain classifier is trained to predict whether a sample came from $\boldsymbol{P}_x$ or $\boldsymbol{Q}_x$. Then, on a held-out mixture of data from $\boldsymbol{P}_x$ and $\boldsymbol{Q}_x$, we compute the domain classifier's accuracy and compare its performance to random chance using a binomial test.

7. Deep Ensemble (Deep Ensemble, [41]) An ensemble of neural networks are trained independently on the entire training dataset using random initialization. A KS test is then performed on the distribution of entropy values computed from each sample in $\boldsymbol{P}$ and $\boldsymbol{Q}$.

B.2 Standard Benchmark Datasets

UCI Heart Disease. The UCI Heart Disease dataset (UCI-HD) [Janosi et al., 1988] includes 76 variables gathered from four distinct patient cohorts located in Cleveland, Hungary, Switzerland, and the VA Long Beach. To reduce the impact of missing data, we focus on nine out of the 14 most frequently used features: age, sex, chest pain type, resting blood pressure, serum cholesterol, fasting blood sugar, resting ECG results, maximum heart rate achieved, and exercise-induced angina. The objective is to predict heart disease diagnosis, measured on a scale from 0 to 4—where 0 denotes no disease and values 1 through 4 indicate increasing severity related to arterial narrowing. Using the proposed setup in [19], the task is binarized, distinguishing between patients with a normal angiographic diagnosis (label 0) and those with any abnormal diagnosis (label greater than 0). The Cleveland and Hungary datasets serve as the ID domain, while Switzerland and VA Long Beach datasets form the deteriorating OOD domain.

CIFAR-10/10.1. The CIFAR-10 image dataset consists of 60,000 color images, each sized 32x32 pixels, divided into 10 different classes such as airplanes, cars, birds, and dogs. The dataset is split into 50,000 training images and 10,000 test images, with each class represented equally. Due to its manageable size and diversity of categories, CIFAR-10 is commonly used for testing and comparing the performance of image recognition models. The CIFAR-10.1 dataset [2] is a test set designed to evaluate how well models trained on CIFAR-10 generalize to new, but similar, data. It consists of 2,000 images collected in a way that closely matches the original CIFAR-10 distribution, but from a separate data source to reduce the risk of overlap or memorization. CIFAR-10.1 was introduced to assess model robustness and identify potential overfitting to the original test set. Despite its similarity to CIFAR-10, many models perform slightly worse on CIFAR-10.1, highlighting the challenge of generalization in machine learning.

The CIFAR-10 dataset is used as the ID dataset with which the mean model of D3M is trained, while the CIFAR-10.1 dataset is considered as a deteriorating shift from CIFAR-10. Thus, we gauge the ability to recognize CIFAR-10.1 as deterioratingly OOD by D3M and its competing baselines.

Camelyon17. The Camelyon17 dataset is a challenging histopathology image classification dataset originally described by [65]. It comprises 327,680 color images (96×96) extracted from lymph node

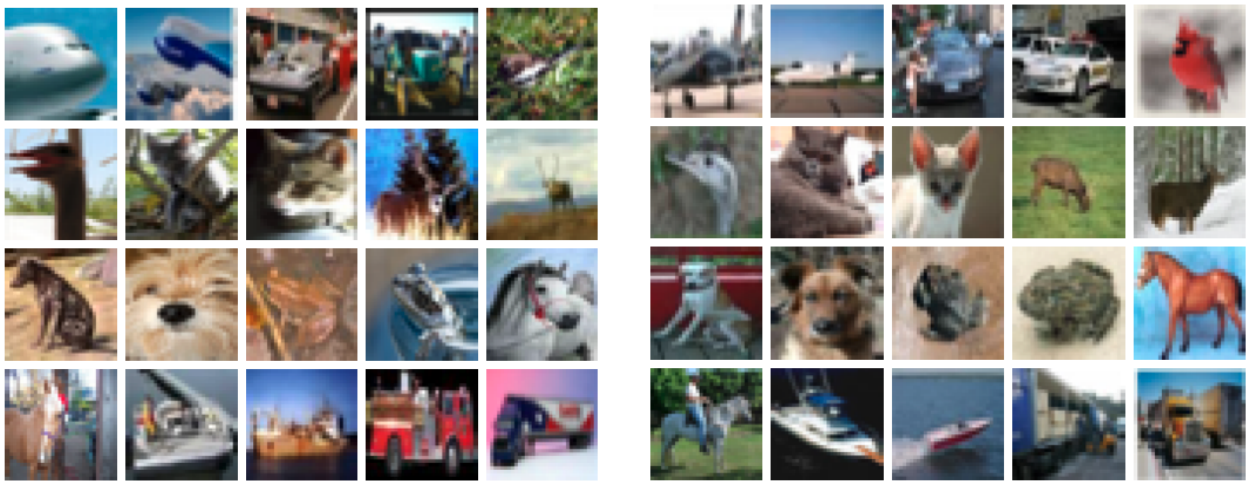

Figure 5: (**Left**) Random samples from CIFAR-10.1. (**Right**) Random samples from CIFAR-10's test set. The images above are borrowed from Recht et. al. "Do CIFAR-10 Classifiers Generalize to CIFAR-10?" [2].

tissue slides, with binary labels indicating the presence of metastatic cancer in the central 32×32 region. Following the WILDS setup, we treat the hospitals from which data was collected as domains: hospitals 1, 2, and 3 are used as source domains for training, while hospital 5 serves as the target test domain. We use the WILDS framework to handle dataset download, preprocessing, and domain partitioning.

B.3 The Internal Medicine (IM) Dataset

Year	Patient Count	Label Ratio
Pre-2017	72316	3.99%
2017H2	17208	3.60 %
2018H1	18233	4.15%
2018H2	18469	3.83%
2019H1	19041	3.50%
2019H2	18601	3.49%
2020H1	15575	4.50%
2020H2	11155	3.48%
2021H1	10625	3.46%
2021H2	7396	2.95%

Table 3: Temporal Split Data Summary

Age	Patient Count	Label Ratio
18-52	33220	0.82 %
52-66	33146	2.36 %
66-72	31048	3.36 %
76 - 85	34055	4.77 %
85+	32399	7.82 %

Table 4: Age Split Data Summary

IM Dataset: Study and Preprocessing. The IM study is a retrospective cohort study of adult patients and their clinical and administrative data.This analysis used data from over 200,000 patients from the IM Database, spanning 7 different hospitals that participated in the IM Study. Each patients information is processed into 900 features including but not limited to: (i) laboratory results and vital results collected up to 48-hours after admission, split into 6 hour intervals, (ii) patient

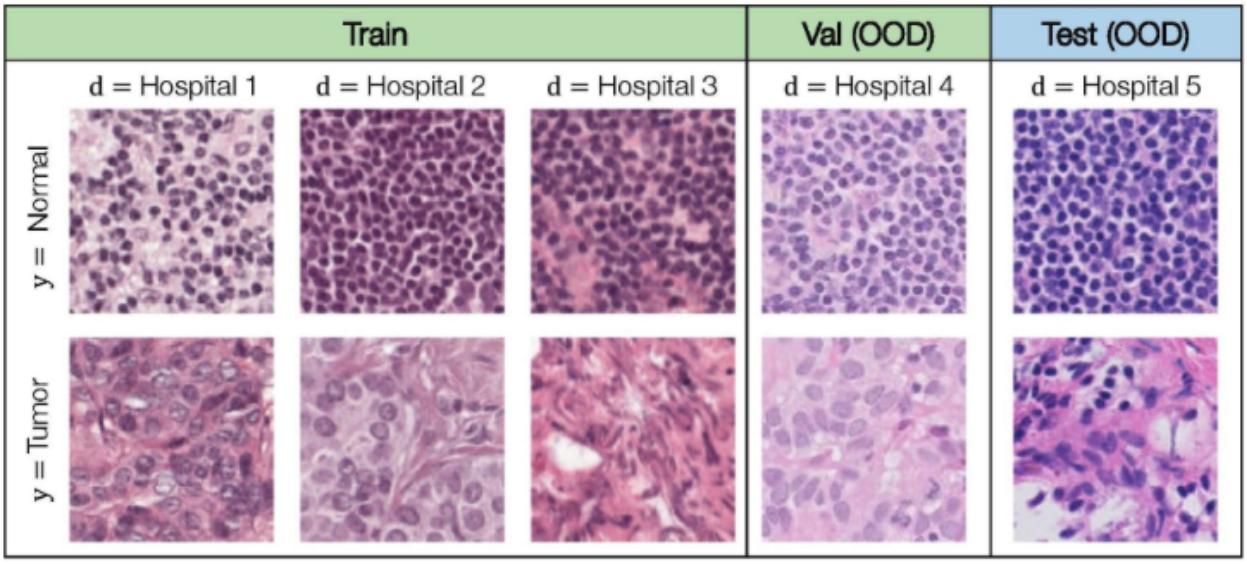

Figure 6: Samples from the Camelyon17 dataset, where hospitals 1, 2, 3 are treated as ID, while hospitals 4 and 5 are deterioratingly OOD. The image above is borrowed from Koh and Sagawa et. al. "WILDS: A benchmark of in-the-wild distribution shifts" [4].

demographic information: age, sex etc, (iii) Patient diagnosis using ICD-10-CA codes. Missing feature values are imputed based on simple averaging. The predictive task related to this data is 14-day mortality for patients based on these collected features.

Data Splitting and Shift. Based on this pre-processed data, 2 shifts are analyzed: (i) temporal shift, and (ii) age-group shift. The temporal shift analysis splits data into half-years - 2018H1, 2019H2, etc. The baseline model uses 2017H1 and prior data for training, and 2017H2 for validation; Tab. 3 shows patient statistics for this split. It is subsequently tested on unseen in distribution data and later splits. The different age groups are created by splitting the data into 5 equally sized groups based on ages of patients: (1) 18-52, (2) 52-66, (3) 66-72, (4) 76 - 85, (5) 85+; Tab. 4 shows patient statistics for this split. The reported analysis trains a baseline model on group 1 (18-52) and then tests on test-sets that contain some portion of data from the 5th group (85+) and the remaining as unseen in distribution data. The portions [0.0, 0.2, 0.4, 0.6, 0.8, 1.0] represent what percentage of the test set is OOD (from group 5), whilst the remaining amount is ID (from group 1). For example a ratio of 0.2 means 20% of the test data is from group 5(OOD) whilst 80% is from group 1(ID). We chose to experiment on such portions instead of just subsequent age groups as this process better displays the TPR of D3M as well as baselines with respect to the degree of shift / performance deterioration.

B.4 Configurations for FE_θ and VBLL_θ

Tabular features. In the tabular setting, we chain affine layers of similar hidden dimension coupled with exponential linear unit (ELU) non-linearities [66]. We use a standard dropout rate of 0.2 across all experiments and employ skip connections between hidden layers. This architecture is used in all experiments with the UCI Heart Disease dataset as well as the IM dataset.

Convolutional features. For CIFAR-10/10.1, we pass the input through an initial convolution and max-pooling, then through a sequence of same-dimension convolutions with batch normalization

[67] and skip-connections. Another max-pool is applied, before the representation is flattened and forwarded through an affine layer to obtain a representation.

For Camelyon17 experiments, we employ pre-trained ResNets [38] and either train from scratch, finetune them during the training of the VBLL$_\theta$ layer, or freeze them while only training the VBLL layer.

Variational Bayesian Last Layers (VBLL). We borrow the implementation from [23] which can be readily coupled with the above neural feature extractors for end-to-end ELBO maximization. In our experiments, we employ the VBLL variant for discriminative classification `vbll.DiscClassification`, and parametrize the covariance matrix of the normal distribution of logits as a diagonal. As for VBLL's hyperparameters, the prior scale and wishart scale hyperparameters are as described in the original manuscript, while we use the **regularization factor** to VBLL to be a factor of n^{-1} where n is the size of the training set. This factor controls the weight of the KL estimate during ELBO maximization at training.

B.5 Sweeping and Hyperparameters

In each experiment, for each test sample size m, we run a hyperparameter sweep in order to identify hyperparameters that (1) achieves the most consistent low FPR when tested in-distribution, and (2) achieves the highest deterioration monitoring TPR. As mentioned previously, the distribution of disagreement rates can be overfitted so that D3M flags **any** sample, regardless of whether they are ID or not, thus justifying the choice of selecting hyperparameters jointly satisfying (1) and (2).

Once the best sets are identified, we run 10 independent seeded runs for each test sample size $m = 10, 20, 50$. We report used hyperparameters in Tables 5 and 6 for transparency and reproducibility. In CIFAR-10/10.1, "Hidden dimension" refers to the dimensionality of the final output of FE$_\theta$, and test size m is identical for D3M and other baseline algorithms for each set of experiments.

Table 5: Hyperparameters for UCI Heart Disease and IM datasets

Group	Hyperparameter	UCI	IM
Train	Learning rate	1×10^{-3}	1×10^{-3}
	Batch size	64	64
	Epochs	50	50
	Weight decay	1×10^{-4}	1×10^{-4}
Model	Hidden dimension	16	128
	Num. hidden layers	4	4
	Dropout	0.2	0.2
VBLL	Regularization factor	100.0	100.0
	Prior scale	1.0	1.0
	Wishart scale	1.0	1.0
D3M	Sampling temperature	1.0	1.0
	Test size m	$10, 20, 50$	200

Table 6: Hyperparameters for CIFAR-10/10.1 and Camelyon17 datasets

CIFAR-10/10.1

Group	Hyperparameter	Value
Train	Learning rate	1×10^{-3}
	Batch size	64
	Epochs	10
	Weight decay	1×10^{-4}
Model	Hidden dimension	256
	Num. mid layers	3
	Initial kernel size	9
	Kernel size	7
	Num. mid channels	128
VBLL	Regularization factor	10.0
	Prior scale	1.0
	Wishart scale	1.0
D3M	Sampling temperature	1.0
	Test size m	$10, 20, 50$

Camelyon17

Group	Hyperparameter	Value
Train	Learning rate	1×10^{-5}
	Batch size	256
	Epochs	2
	Weight decay	1×10^{-4}
Model	ResNet type	ResNet34
	From pretrained	True
	Freeze features	True
VBLL	Regularization factor	100.0
	Prior scale	5.0
	Wishart scale	2.0
D3M	Sampling temperature	2.0
	Test size m	$10, 20, 50$

Common to all setups. For all experiments, the number of posterior samples K is set to 5000, the size of the empirical distribution of maximum disagreement rates $|\Phi|$ is set to 1000. For each experiment, once **Train** and **Calibrate** is completed, we deploy the model on 100 independent samplings of the questionable test data. If model deterioration occurs (this is the case for the standard benchmark experiments as well as the IM dataset *temporal* shift experiment but not the IM dataset *age* shift experiment), we report the number of times D3M flagged these deteriorating samples out of 100 as TPR. Finally, confidence statistics are aggregated and computed on TPRs reported from seeded, independent **Train-Calibrate-Deploy** D3M cycles. All optimization is done using AdamW [68]. Finally, we start seeded, independent, identical runs beginning at seed = 57 since it is our favorite prime number, and increase seed by +1 for each run.

Only reporting TPRs of runs achieving low FPR. Importantly, we aggregate only TPRs achieved when a FPR below 0.10 in-distribution is achieved. This FPR is calculated on a held-out ID validation set that D3M has not yet seen during **Train** nor **Calibrate**. Therefore, for all experiments we run seeded runs until 10 runs recording ID FPR below 0.10 are found, and their TPR statistics are computed, as certain runs do not achieve the ID FPR tolerance desired.

When deploying D3M in a real-world healthcare setting, for instance, upon the completion of the **Calibrate** step, one could imagine validating this calibration step by computing an ID FPR score, independent of deployment. IF this ID FPR score is higher than a tolerated threshold α, the practitioner could either increase the size of Φ to eliminate noise from sampling, or consider finding another set of hyperparameters that would lead to more stable calibration.

B.6 Additional D3M Results on Standard Benchmark

We further tested D3M on 100 and 200 calibration/test samples on the same set of hyperparameters above. Table 7 summarizes our findings.

	UCI Heart Disease		CIFAR 10.1		Camelyon 17	
	100	200	100	200	100	200
D3M (Ours)	**.93±.10**	**.99±.01**	**.91±.11**	**.99±.01**	**1.0±.00**	**1.0±.00**

Table 7: True positive rates (TPR) for D3M across datasets and test sizes $100, 200$.

At higher test sizes, D3M achieves near-perfect TPR. This is consistent across all experiments. This suggests that D3M could be an effective tool to monitor model deterioration. However, of note is that for test size 100, in the UCI Heart Disease and CIFAR-10/10.1 experiments, D3M is still logging unusually high standard deviation, where we suspect the noise to be coming from the sampling procedure from the VBLL_θ distribution of logits.

Trading off deployment-time computations with sweeping D3M is efficient when comparing to other disagreement-based detection and monitoring algorithms. However, the method is inherently noisier due to several levels of approximation to its idealized version (Algorithms 1 and 2). In particular, we found that D3M is **sensitive to the choice of hyperparameters** in order to achieve great performance. Therefore, the payment of computational cost is carried through prior to deployment in the sweeping itself, rather than during deployment as is done in [19]. We argue, however, that this is **preferable in edge deployment scenarios**, such as in hospitals or embedded systems, where real-time responsiveness and resource constraints are critical by front-loading the computational burden during the sweeping phase. One can imagine that for an AI terminal as part of a hospital computational infrastructure for instance, the ability to perform robust detection and monitoring with minimal overhead at deployment time significantly enhances reliability and usability in practice.

B.7 Statement on the Usage of Computing Resources

All experiments were run on High Performance Computing (HPC) clusters.

UCI Heart Disease. UCI Heart Disease experiments were run on GPU nodes with at minimum 8GB of GPU memory, 6 CPU cores, and 8GB RAM. The total runtime of D3M prior to deployment is less than 5 minutes.

CIFAR-10/10.1. CIFAR-10/10.1 experiments were run on GPU nodes with at minimum 24GB of GPU memory to accomodate the largest configurations of convolutions, 12 CPU cores, and 12GB RAM. The total runtime of D3M prior to deployment is less than 10 minutes.

Camelyon17. Camelyon17 experiments were run on GPU nodes with at minimum 80GB of GPU memory to accomodate the largest ResNets during sweeping, 12 CPU cores, and 12GB RAM. The total runtime of D3M prior to deployment is less than 1 hour.

IM Dataset. Experiments on the IM datset were run on GPU and CPU nodes. We request at minimum 16GB of GPU memory (when applicable), 9 CPU cores, and 32GB of RAM. The total runtime of D3M prior to deployment is less than 1 hour. Although models for IM were significantly smaller than vision models for Camelyon17 and CIFAR-10/10.1, due to the number of samples available as well as older CPU hardware, the runtime was significantly extended.